

The marriage of Xenes and hydrogels: Fundamentals, applications, and outlook

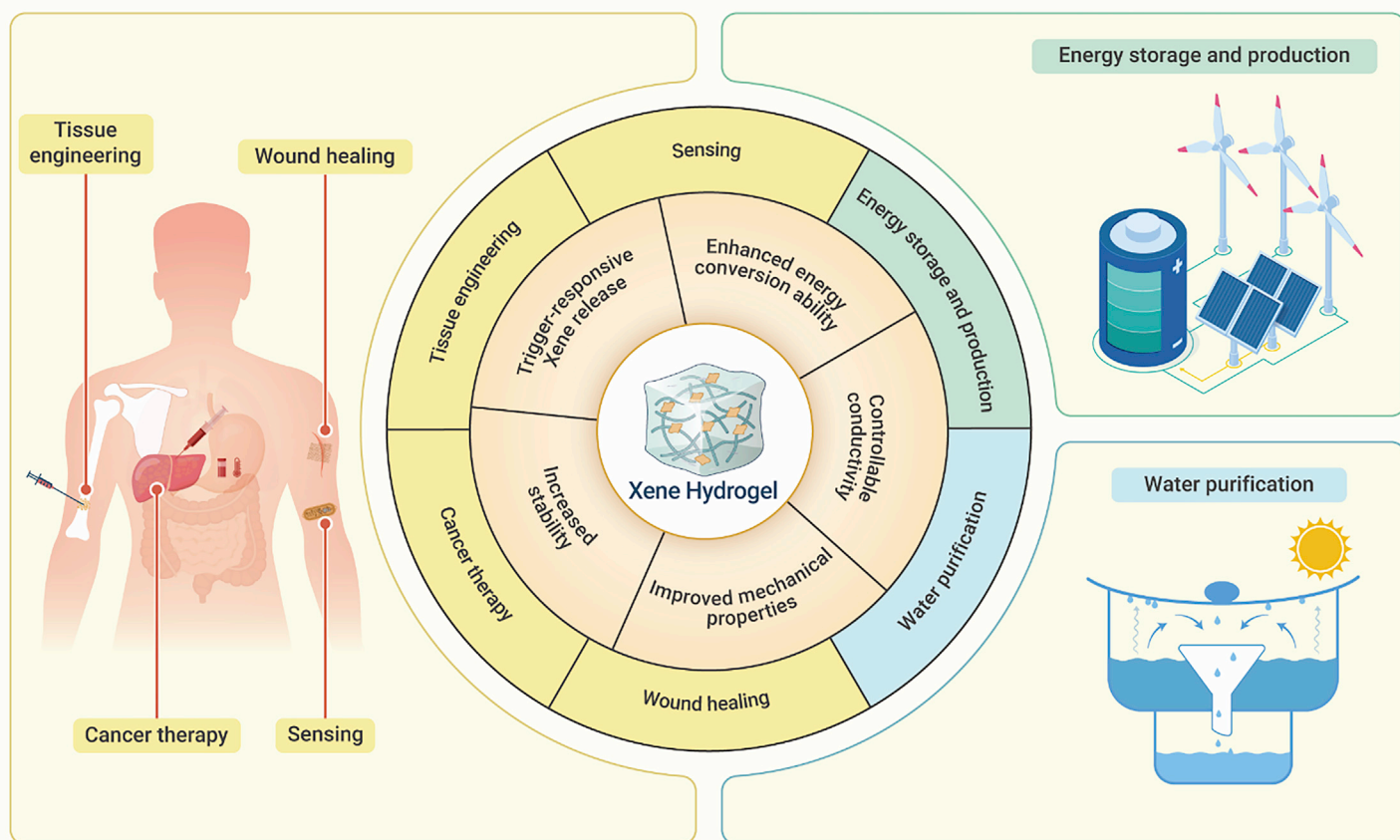
Yong Kang,^{1,5} Hanjie Zhang,^{4,5} Liqun Chen,¹ Jinrui Dong,¹ Bin Yao,¹ Xue Yuan,¹ Duotian Qin,² Alexey V. Yaremenko,² Chuang Liu,² Chan Feng,^{2,3,*} Xiaoyuan Ji,^{1,2,*} and Wei Tao^{2,*}

*Correspondence: chanfeng_zju@163.com (C.F.); jixiaoyuan@tju.edu.cn (X.J.); wtao@bwh.harvard.edu (W.T.)

Received: June 13, 2022; Accepted: September 19, 2022; Published Online: September 22, 2022; <https://doi.org/10.1016/j.xinn.2022.100327>

© 2022 The Author(s). This is an open access article under the CC BY-NC-ND license (<http://creativecommons.org/licenses/by-nc-nd/4.0/>).

GRAPHICAL ABSTRACT



PUBLIC SUMMARY

- Two-dimensional mono-elemental nanosheets (Xenes) endow tunable application
- Synthesis mechanism, properties, and applications of Xene hydrogels are summarized
- Expanding performance and applications of both hydrogels and Xenes are presented



The marriage of Xenes and hydrogels: Fundamentals, applications, and outlook

Yong Kang,^{1,5} Hanjie Zhang,^{4,5} Liqun Chen,¹ Jinrui Dong,¹ Bin Yao,¹ Xue Yuan,¹ Duotian Qin,² Alexey V. Yaremenko,² Chuang Liu,² Chan Feng,^{2,3,*} Xiaoyuan Ji,^{1,2,*} and Wei Tao^{2,*}

¹Academy of Medical Engineering and Translational Medicine, Medical College, Tianjin University, Tianjin 300072, China

²Center for Nanomedicine and Department of Anesthesiology, Brigham and Women's Hospital, Harvard Medical School, Boston, MA 02115, USA

³Department of Respiratory Medicine, Sir Run Shaw Hospital, Zhejiang University School of Medicine, Hangzhou, Zhejiang 310016, China

⁴Tianjin Key Laboratory of Biomedical Materials, Key Laboratory of Biomaterials and Nanotechnology for Cancer Immunotherapy, Institute of Biomedical Engineering, Chinese Academy of Medical Sciences and Peking Union Medical College, Tianjin 300192, China

⁵These authors contributed equally

*Correspondence: chanfeng_zju@163.com (C.F.); jixiaoyuan@tju.edu.cn (X.J.); wtao@bwh.harvard.edu (W.T.)

Received: June 13, 2022; Accepted: September 19, 2022; Published Online: September 22, 2022; <https://doi.org/10.1016/j.xinn.2022.100327>

© 2022 The Author(s). This is an open access article under the CC BY-NC-ND license (<http://creativecommons.org/licenses/by-nc-nd/4.0/>).

Citation: Kang Y., Zhang H., Chen L., et al., (2022). The marriage of Xenes and hydrogels: Fundamentals, applications, and outlook. *The Innovation* 3(6), 100327.

Hydrogels have blossomed as superstars in various fields, owing to their prospective applications in tissue engineering, soft electronics and sensors, flexible energy storage, and biomedicines. Two-dimensional (2D) nanomaterials, especially 2D mono-elemental nanosheets (Xenes) exhibit high aspect ratio morphology, good biocompatibility, metallic conductivity, and tunable electrochemical properties. These fascinating characteristics endow numerous tunable application-specific properties for the construction of Xene-based hydrogels. Hierarchical multifunctional hydrogels can be prepared according to the application requirements and can be effectively tuned by different stimulation to complete specific tasks in a spatiotemporal sequence. In this review, the synthesis mechanism, properties, and emerging applications of Xene hydrogels are summarized, followed by a discussion on expanding the performance and application range of both hydrogels and Xenes.

INTRODUCTION

Hydrogels are three-dimensional (3D) networks composed of gelators and water and are suitable for applications in the water phase.^{1,2,3} The gelators of typical hydrogels are hydrophilic polymers exhibiting distinguishing properties of swelling, transmittance, softness, biocompatibility, and ease of modification.⁴ Both market and scientific research data confirmed the practical value of hydrogels in daily life and the biomedical fields, i.e., diapers and wound dressing.^{5,6} However, the interactions between hydrogel polymers are weaker to maintain the ductility and stability. Interacting with other materials, hydrogels mainly offer attachment points and spaces rather than disposing of adsorbed cargos due to inertness, limiting hydrogels' applications in established fields.⁷ To overcome these limitations, different materials are incorporated into the hydrogel matrix.^{8–13} The increased crosslinking points can improve the mechanical properties of the matrix. In addition, functional materials such as molecules, polymers, and inorganic particles offer other exceptional features, such as nourishment, disease treatment, dye degradation, sterilization, and electrical conductivity.^{14–17}

The involvement of two-dimensional (2D) materials is an effective method to improve the properties and expand the hydrogel applications, owing to the confined carrier migration and heat diffusion in a 2D plane.^{18,19} A class of 2D mono-elemental materials with a similar structure to graphene is defined as Xenes. Xs are elements of the IIIA–VIA groups in the periodic table (Figure 1) and the corresponding Xenes are graphene, arsenene, germanene, boronene, antimonene, silicene, and stanene. Although X can be nonmetals (carbon, phosphorus, and selenium), metalloids (boron, silicon, germanium, arsenic, antimony, and tellurium), and metals (gallium, tin, and bismuth), most Xenes exhibit a metallic property, not exactly corresponding to their bulk materials. As 2D materials, Xenes show outstanding physical and chemical reactivity due to their atomic out-of-plane thickness and attain special electrical, photonic, magnetic, and catalytic properties. Due to their mono-elemental composition, Xenes show superior performance and a wide range of applications, compared with other 2D materials. First, the hybridized forms of X atoms in Xenes are sp^2 or sp^3 , i.e., indicating limited covalent bonding modes between identical atoms, making Xenes structures simple, predictable, controllable, and appreciable. Second, Xenes properties can be tuned by changing the structure; i.e., layer number²⁰ or transformation to another allotrope.²¹ Also, the simple composition ensures limited and innocuous degradation products, contributing to high environmental and biological compat-

ibility. Further investigations on these simple Xenes can lead to some fascinating research on other 2D materials.

The restrained reactions in two dimensions and lack of stability of Xenes in an embedded 3D matrix are some limitations; therefore, several strategies have been designed for improved dispersion and extended applications.²² Recently, emerging 2D Xenes are introduced in hydrogel networks. Three-dimensional hydrogels can serve as a scaffold for 2D Xenes and enhance the properties and applications of hydrogels. In this review, the gelation mechanism, properties, and emerging applications of Xene-based hydrogels are summarized, focusing on the expanding performance and application range of hydrogels and Xenes in different fields.

XENE HYDROGELS: DESIGN AND ASSEMBLY

The synthesis of Xenes and hydrogels has been well developed and discussed as the basic steps for Xene hydrogel preparation.^{23,24} Figure 2 shows the simplified process for the synthesis of hydrogel and Xene. Sonication-assisted liquid-phase exfoliation is used to obtain phosphorene,²⁵ arsenene,²⁶ and germanene,²⁷ from the layered bulk materials. Other top-down methods include chemical exfoliation²⁸ and mechanical exfoliation.²⁹ In addition, liquid exfoliating and thermal oxidation etching are coupled to prepare ultrathin borophene.³⁰ Conversely, the construction of Xenes via bottom-up strategies refers to the preparation from atoms/ions, and the methods include physical vapor deposition and chemical vapor deposition. These methods increase Xene categories without referring to the lattice of bulk materials.^{31–34} Similarly, methods for hydrogel preparation are based on covalent linkages or noncovalent interactions (hydrogen bonding, electrostatic, and hydrophobic forces) among polymers, including freeze-drying, freeze/thaw cycling, self-assembly, small molecule/ionizing radiation/free radical-induced covalent crosslinking, etc.^{35,36} In the last few years, hydrogels are also fabricated by modern technologies such as electrostatic spinning and 3D bioprinting.^{37–39}

During Xene hydrogel fabrication, precise control of the interactions between Xenes and hydrogels is required to bring out the desired advantages of both components. For instance, in photocatalytic degradation, the adsorption ability of graphene hydrogel for target pollutants increases with the addition of graphene oxide (GO). However, a high concentration of GO severely restricts light penetration and limits photocatalytic efficiency.⁴⁰ Also, the stability of Xenes during the preparation process is also maintained by coating other materials on the surface.⁴¹ Xene hydrogels are also fabricated by incorporating two components in different orders and methods, displaying fundamental differences in the interaction between polymers and Xenes, the architectural organization of the final Xene hydrogel network, and their practical applications. Accordingly, there are two main procedures: (1) Xene incorporation in crosslinked hydrogels (Figure 3A), and (2) hydrogel crosslinking in the presence of Xenes (Figure 3B). Xenes can also gelatinize without polymers, i.e., self-gel of Xenes (Figure 3C). The basic steps of the three manufacturing processes with their principles, as well as the advantages and challenges, are also discussed in the following sections.

Xenes incorporation in crosslinked hydrogels

Benefiting from the hydrogel's porous structure and its ability to incorporate smaller-sized particles, the pre-prepared Xenes can be loaded to crosslinked hydrogel networks (Figure 3A). The most common procedure relies on hydrogel

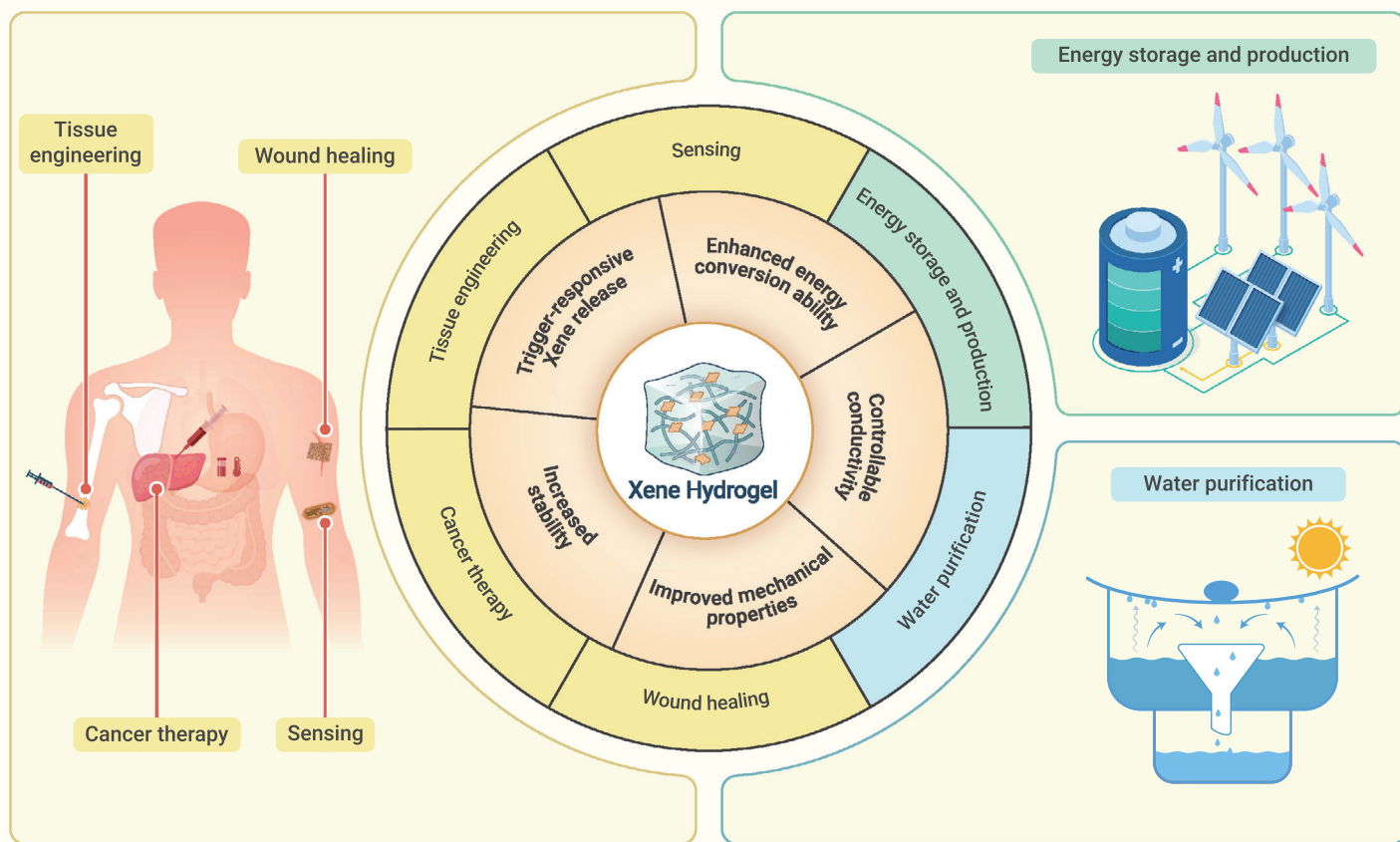


Figure 1. Reported elements (with color background) that can form Xenos Blue background, metals; green background, metalloids; yellow background, nonmetals. White background, unreported yet.

swelling in concentrated Xene solutions where the gelatinous composite is non-responsive to the Xene embedding conditions. Xenos can diffuse into the injectable hydrogel pores in the solution. For example, hydrogels containing black phosphorus (BP) via hypodermic injection, constructed with hyaluronic acid (2 wt%) and pluronic F-127 (25 wt%), are beneficial to inhibit tumor recurrence after surgery.⁴² Germanene-based hydrogels are developed by mixing germanene with hydrogel composed of chitosan and agarose.²⁷ Hydrogels can also have a fixed shape. Li et al. reported a sandwiched BP hydrogel by synthesizing a layer of chitosan-based hydrogel and then loading BP nanosheets onto the chitosan layer with a syringe filter. Subsequently, another hydrogel layer is equipped with the BP-coated chitosan hydrogel.⁴³

These methods are not suitable for Xenos with strong interactions, since strategies for increasing dispersibility may impair some properties of Xenos. For example, graphene is highly hydrophobic that is not evenly dispersed in an aqueous solution and hydrogels. In practical applications, a uniform distribution of graphene hydrogels is achieved by anchoring the surface with polar functional groups, including hydroxyl and carboxyl, through chemical modification of oxidation or reduction. Unfortunately, the covalent functionalization can destroy the original lattice of graphene, resulting in altered properties, especially electric conductivity, and both reduced graphene and GO exhibit lower conductivity than original graphene. Although GO is reduced again, only one-third of the conductivity can be restored.⁴⁴ *In situ* Xenos formation after hydrogel crosslinking can significantly avoid undesired self-aggregation of Xenos.

Hydrogel crosslinking in the presence of Xenos

One of the most preferred methods to manufacture hybrid Xene hydrogels is to combine Xene suspensions with hydrogel precursors before hydrogel formation (Figure 3B). Typically, this process can realize relatively homogeneous incorporation of Xenos in hydrogel compared with other techniques, allowing the incorporation of various Xenos since Xenos are pre-synthesized before hydrogel crosslinking. The challenges in this approach involve the requirement of a good uniform dispersion ability and the requirement of an appropriate concentration

of Xenos affecting the distribution of Xenos and hydrogel network formation. The simplest gelation method is dissolving Xenos into polymer solutions and removing the solutions by heating^{45,46} or freezing-thawing cycles.^{47–49} Also, thermal,^{50–52} radiation,⁵³ pH variation,^{54,55} or chemical cross-linkers^{56–60} are commonly used to fabricate Xene hydrogels. For example, BP@hydrogel was prepared by mixing the agarose solution with BP sheets under mechanical stirring for 30 min at 90°C and stored at 4°C for 30 min.⁶¹ Liang et al. prepared homogeneous graphene/PVA solution by gradually adding GO/H₂O solution to the PVA solution at 40°C and then sonicating for 30 min. Then, the mixture was poured into a Teflon petri dish and dried at 60°C for GO/PVA hydrogel film formation.⁴⁵

Xenos are also suitable crosslinking nodes in 3D platforms. Benefiting from the advances in polymer chemistry, the selective functional groups with target complementary moieties are engineered onto the Xenos' surface, thus achieving augmented interactions in hydrogel precursors, then preparing nanocomposite hydrogels via interdependent assembly. Meanwhile, such Xene hydrogel interactions possess high flexibility and adaptability to encode nanocomposites in the final hybrid structure. For example, polydopamine-coated BP was attached to polymer hydrogel via noncovalent interactions with GelMA, including hydrogen bonds and π - π stacking.⁴¹ Liu et al. synthesized graphene peroxide (GPO), which decomposed into free radicals (GO•, OH•) on heating. They dissolved acrylamide in GPO aqueous dispersion, sealed the sample into glass molds, and heated it in a water bath at 45°C to form hydrogels.⁶²

Self-gel of Xenos

In 2008, Li et al. reported a chemically converted graphene (CCG) that could stably disperse in water without any surfactants (Figure 3C).⁶³ Exfoliated graphite oxide dispersions were first synthesized and then directly converted to stable graphene colloids through hydrazine reduction under specific conditions. Later in 2011, the same group found that CCG sheets can self-gel at the solid-liquid interface via the face-to-face method during filtration when the vacuum was applied; therefore, a layer of water molecules was tightly captured by the oxygen-containing groups on the CCG surface. This kind of directional

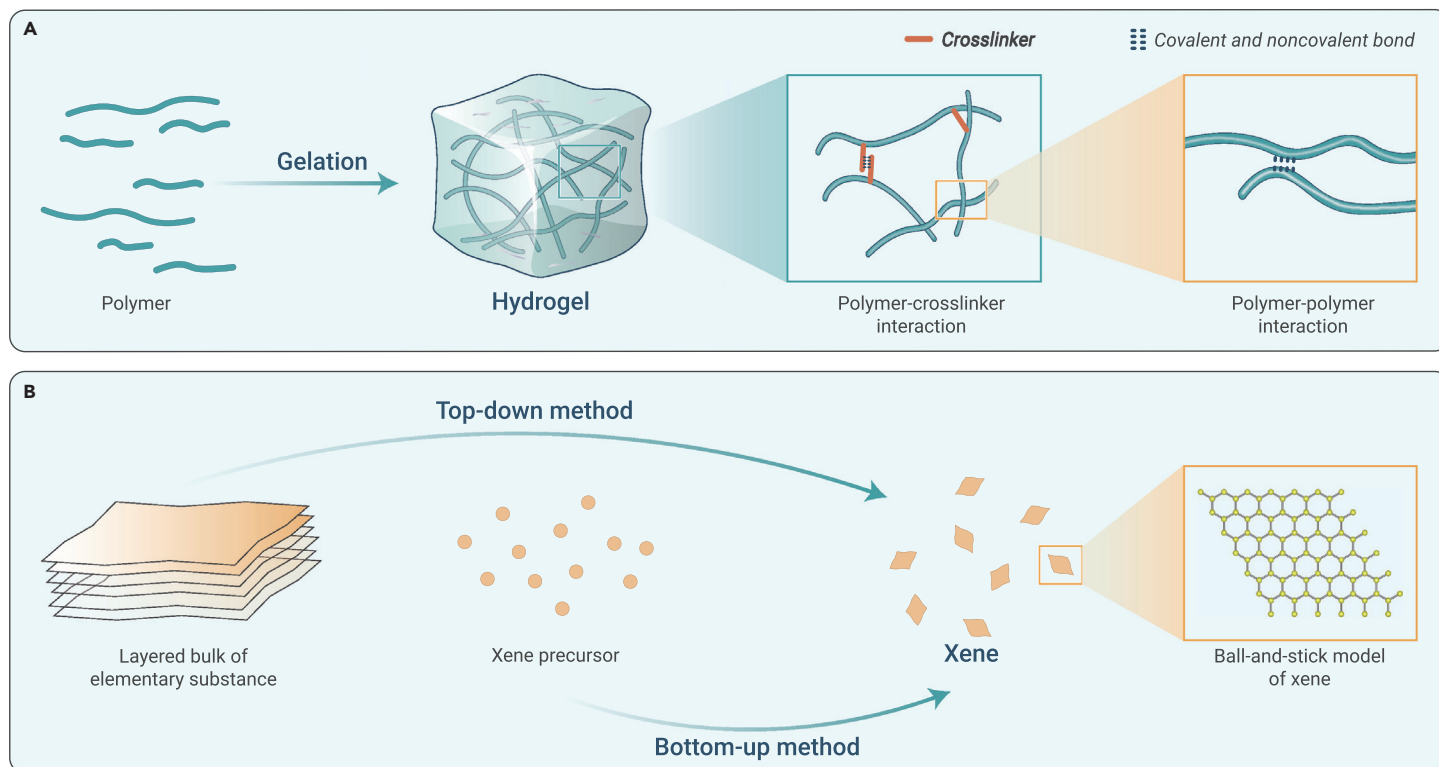


Figure 2. Brief synthesis process and structure of hydrogel and Xene, respectively (A) Traditional hydrogels are fabricated by polymers and water via a process called gelation. Crosslinkers can be used to connect polymer chains. And covalent and noncovalent bonds also contribute to the 3D mesh development. (B) Xenes can be synthesized via two methods. The top-down method always requires a layered structure of bulk materials and uses techniques to break the interlayer forces. The bottom-up method takes no account of the bulk structure, synthesizing Xenes from their precursors. Most Xenes have a two-dimensional honeycomb lattice.

conductive hydrogel film demonstrated unprecedented electrical, mechanical, and anisotropic stimuli-responsive properties.⁶⁴ Moreover, during self-gelation, a second Xene can *in situ* grow on the original Xene to form the composite hydrogel.⁶⁵

PROPERTIES AND INTERACTIONS OF XENES AND HYDROGELS

The integrated Xene hydrogels display the properties of both components and additional features associated with the interactions between Xenes and hydrogels (Figure 4). In this section, the most fundamental properties of polymer hydrogels and Xenes are discussed, based on their interactions. Furthermore, the influence of hydrogels on Xenes and the increased/new features of Xenes-based hydrogels for further applications are described.

Fundamental properties of hydrogels and Xenes

For hydrogels. Hygroscopicity and swelling property. Hydrogels contain several hydrophilic groups, such as -OH, -CONH-, -CONH₂, and -SO₃H; therefore, obtained hygroscopicity and swelling properties promise their utilization in diapers, wound dressing, and swelling-related sensors.

Mechanical properties. The water content and crosslinking concentration can influence the mechanical behaviors of hydrogels, especially the plasticity and toughness, endowing them with various shapes to adapt to different applications. Pure hydrogels always show brittleness, which limits their practical applications.

Biocompatibility. Good biocompatibility mainly depends on two aspects. First, many hydrogels rapidly degrade in the body, eliminating the risk of any serious hepatotoxicity and nephrotoxicity. For example, Li et al. developed a biodegradable photothermal hydrogel for photothermal therapy (PTT). The hydrogel was composed of aldehyde-modified dextran through imine bond formation. After injecting it into the tumor tissue, it degraded over time, demonstrating good biocompatibility.⁶⁶ Second, the unique characteristics of hydrogel also determine its good biocompatibility. The low interfacial tension between hydrogels and aqueous fluids, due to high-water content reaching 99% in some cases, leads to weak adhesion of hydrogels to proteins and cells. It also imparts softness properties to living tissue; hence, showing good biocompatibility with blood, body fluid, and human tissue. Many studies have confirmed that most hydrogels are biocompatible.⁶⁷

Porosity. The 3D mesh structure of hydrogels offers anchors and spaces for other materials, to deliver or adsorb cargos, such as loading substances with specific functions, like therapeutics,^{68,69} enzymes,^{70,71} nanoparticles,⁷² and nanosheets.^{73,74}

Transparency. Most hydrogels are so transparent that they hardly affect the optical properties of their contents. Therefore, several concentration-related hydrogel sensors were developed due to photorefractive variation.⁷⁵

Adjustability. The hydrogel structure and properties can be altered by the water content, crosslinking concentration, additives, and environment. Additives can impart more features, further extending the applications of hydrogels.

Stability. When the crosslinking of hydrogel networks is through noncovalent physical interactions, the change in nanoscale structure and water content occurs with environmental change.^{76,77}

For Xenes. Seven properties of Xenes influencing their application are listed below. Since Xenes contain a wide range of 2D mono-elemental materials, therefore, several unique properties of these materials are observed, such as high stability, tunable band gap, photothermal conversion efficiency, catalytic ability, and electrical properties (Table 1).

Layered structure. Controlling the synthesis of Xenes can effectively change the layer number of obtained Xenes, which alters the band gap size and conductivity of Xenes.²⁰ Due to layered structure, Xenes have large surface areas with exposed atoms, physically or chemically interacting with other materials. These interactions can be used for further modification, cargo delivery, and several other applications.

Stability. Xenes exhibit variable stability. Borophene,³⁰ gallenene,⁸³ and antimone^{114,115} are relatively stable under atmospheric conditions. However, the active surface can damage the stability of Xenes by aggregation or degradation in the environment. With a layered structure, the bare 2D nanosheets are likely to stack together through strong *van der Waals* interactions and π - π stacking, thereby, covering the surfaces, decreasing active sites, and even impairing electrical, optical, and other properties of graphene and stanene.^{86,100} Germanene can degrade rapidly.^{95,96} Similarly, silicene,⁹⁰ phosphorene,^{25,127} arsenene,^{110,128} bismuthene,¹¹⁹ selenene,¹²³ and tellurene¹²⁵ are biodegradable, further affecting the properties and even functions.

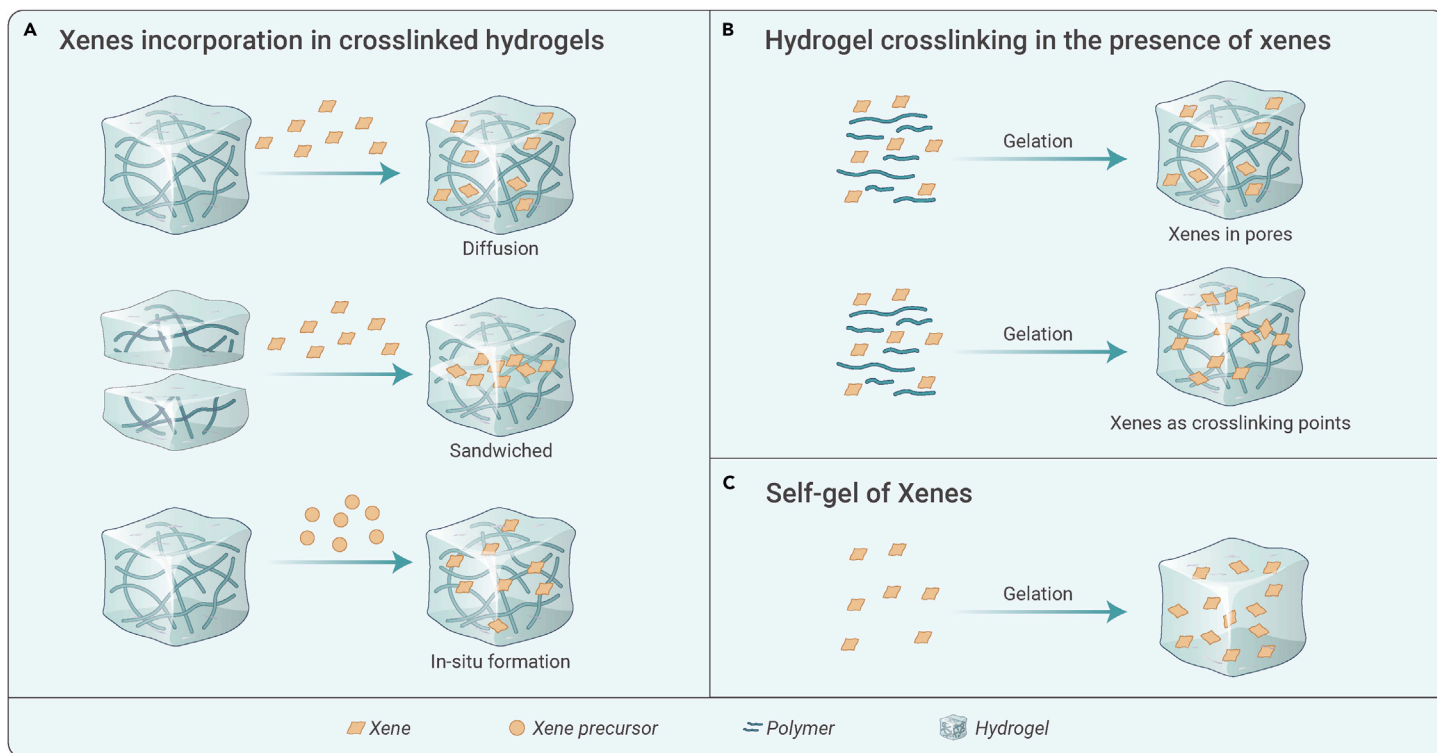


Figure 3. Synthesis of Xene hydrogels via three different methods (A) Xenes incorporation in crosslinked hydrogels, (B) hydrogel crosslinking in the presence of Xenes, and (C) self-gel of Xenes.

Environmental and biological compatibility. The degradation of the single element Xenes is more obvious in the environment or *in vivo* than in other 2D materials, and some Xenes are biodegradable with innocuous metabolites, enhancing their potential in environmental and biomedical applications.¹²⁹

Tunable band gap. The band gaps of Xenes can be adjusted by the number of layers, surface modification, and external physical triggers, influencing the carrier mobility, thermal conductivity, and other electrical properties.¹²⁰ Among these materials, phosphorene,⁷⁸ arsenene, antimonene,¹¹¹ and tellurene¹²⁶ have layer-dependent band gaps. For example, BP nanosheets have thickness-dependent band gaps, in the range of 0.3 eV and 2 eV, obtained by adjusting the thickness of nanosheets.¹³⁰ Some Xenes have zero or near-zero band gaps,⁷⁸ such as borophene, gallenene, graphene, and silicene. The band gap of silicene can be tuned under a vertical electric field⁹¹ and that of borophene can be increased by hydrogenation/fluorination or a shear strain.⁷⁹ Similarly, the band gap of germanene and stanene can be tuned under a perpendicular electric field.^{91,101}

Photothermal conversion ability. Some 2D Xenes have a direct and adjustable bandgap with light conversion efficiency.^{91,104,131,132} Due to the supereminent light absorption and conversion efficiency, Xenes are applied in photoacoustic imaging, PTT, and photodynamic therapy (PDT). For example, borene with distinguishing photothermal conversion efficiency has been reported to attain 42.5% much higher than that of Au nanoparticles, and 13.1% for PDA.^{30,133} In addition, graphene,⁸⁷ stanene,¹⁰⁰ antimonene,¹¹⁶ and tellurene¹²⁵ have 40% higher photothermal conversion efficiency, which makes these materials excellent photothermal agents for PTT.

Catalytic ability. Owing to a suitable band gap, some Xenes respond to external triggers (light or mechanical stress) to catalyze adsorptive substances, such as consuming H₂O to produce O₂ and CO₂ to formate. Except that the catalytic ability of gallenene, selenene, and tellurene has not been reported yet, other Xenes can catalyze energy generation reactions and other applications.^{80,88,89,92,93,97,102,105–108,112,117} For example, Cao et al. prepared an atomic thin layer of bismuthene with an average thickness of 1.28–1.45 nm. The obtained materials had a large number of exposed active centers, which significantly improved the CO₂ reduction performance and showed long-term stability in the electrochemical conversion of CO₂ to formate.¹²¹

Electrical property. As a honeycomb lattice structure, most Xenes are topological insulators to harness a quantum-mechanical property of spins to conduct electricity.¹³⁴ Borophene,^{81,82} gallenene,^{84,85} graphenes,⁷⁸ and silicene⁹⁴ exhibit

high electrical conductivity, and other Xenes are semiconducting as well.^{98,103,109,113,118,122,124} Some Xenes possess a metallic-to-semiconductor transforming character with the change in thickness,¹¹¹ applied stress,¹³⁵ or annealing temperature.⁹⁹ For example, Chen et al. fabricated germanium sheets, revealing the low electrical conductivity of germanium, consistent with the larger band gap. After heat treatment, the electrical conductivity increased sharply and the material was converted from insulator to metal.⁹⁹ As a result, the conductivity and semi-conductivity of different Xenes can be used in hydrogel structures.

Influence of gelation on Xene properties

Increased stability. The well-sized holes and attachable groups in hydrogels can keep additives at a specific distance to maintain the structural and functional stability of hybrid hydrogels, thus reducing Xene aggregation and displaying steady and continuous function.⁶⁷

Hydrogel-controlled Xene release. The structure of some hydrogels can change with the external environment, resulting in cargo release. This aspect is particularly suitable for drug delivery applications.¹³⁶

Increased conductivity. Self-gel can integrate scattered Xenes with increased electrical conductivity and initial discharge capacity.⁶⁵

Xene-induced/enhanced properties in hydrogels

Increased toughness and stiffness. On account of abundant water content, conventional hydrogels have the disadvantages of lower mechanical properties, limiting their applications in many fields. The adulteration of Xenes improves the tensile strength of the hydrogel.^{137,138} For instance, Ye et al. introduced GO sheets into the poly(acrylic acid) hydrogels (BIS-gel) and increased the mechanical performance.¹³⁹ The hydrogel without GO sheets readily broke and its elongation was just 70%. However, the GO-BIS-gel showed excellent ductility and could even be knotted with elongation at break was close to 300%. Zhang et al. fabricated graphene oxide/polyacrylamide (GO/PAM) hydrogels as actuator devices via *in situ* polymerization.¹⁴⁰ The compressive strength of as-synthesized hydrogels increased significantly with GO content, and it was about six times stronger than pure PAM hydrogel at 1% GO content.

Increased conductivity. The conductive properties of hydrogels are not particularly high, and these can be increased by the addition of Xenes. For example, the electrical impedance values dramatically decreased to 12 k Ω after BP loading, while that of GelMA hydrogel was 46 k Ω .⁴¹ Compared with

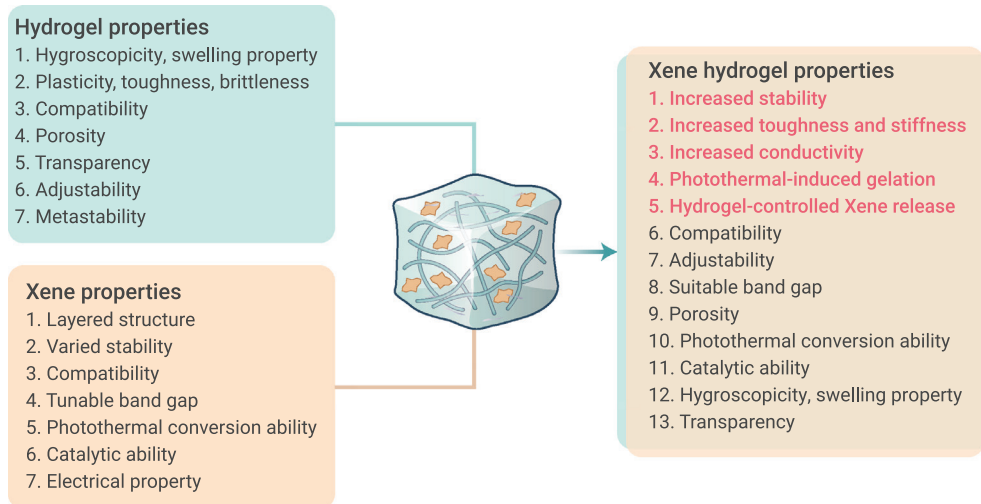


Figure 4. Properties of hydrogel, Xene, and Xene hydrogel

electroconductive hydrogels obtained from the conductive polymers and highly hydrated hydrogels, Xene hydrogel exhibited poor conductivity due to the simple embedding of Xenes into the hydrogel while conductive polymers were blended with the hydrogel matrix to form a continuous conducting 3D structure. In addition, Xenes are not always evenly distributed in hydrogels, which can impair the conductivity of hybrid hydrogels.¹⁴¹

Photothermal conversion ability. Conventional hydrogels show distinct energy conversion characteristics after the incorporation of Xenes. Wang et al. constructed CS/AM NSs composite hydrogels with distinguished photothermal properties by introducing antimonene nanosheets (AM NSs) into chitosan.¹⁴² Under 808-nm laser irradiation with the intensity of 1.5 W cm^{-2} , the temperature of the CS/AM NSs hydrogel increased by 30°C within 10 min, while the temperature of that without AM NSs almost remain unchanged.

Photothermal-induced gelation. The photothermal function of Xenes also provides a stimulus resource to design stimuli-responsive hydrogels. Gao et al. fabricated an injectable thermo-responsive BP NSs-based chitosan hydrogel, which was liquid at room temperature.¹⁴³ Under the laser irradiation (wavelength 808 nm and intensity 1.0 W cm^{-2}), BP NSs converted light energy into heat energy and rapidly solidified the thermosensitive hydrogel.

APPLICATIONS OF XENE HYDROGELS

Although Xenes and hydrogels have been already used in many fields,^{144–148} the combination of these two materials expands their applications due to the increased and enhanced properties. Specifically, Xene hydrogels have been used in biomedical, sensing, energy, and environment, as shown in Table 2. In this part, we explore the current applications of hybrid Xene hydrogels.

Biomedical application

Due to adjustable mechanical properties, exceptional electrical and optical features, biocompatibility, and biodegradability, Xene hydrogels are widely used in the biomedical field, including cancer therapy, tissue engineering, and wound healing (Figure 5). In Xene hydrogel, Xenes are always functional components, and hydrogels are scaffolds. In addition, Xene hydrogels are suitable for designing delivery systems owing to their excellent cargo-loading capacity and controllable release. The pores in hydrogels provide ample spaces and Xenes are characterized by broad surface area and unique surface properties.¹⁶¹ In addition, due to their excellent biocompatibility, soft structure, and appropriate mechanical strength, the hydrogels are tuned into various dosage forms for drug delivery and controlled drug release through nasal delivery, oral delivery, transdermal and subcutaneous injection, and so on.¹⁶² For example, BP has a conjugate structure with a negative zeta potential of about -25 mV . These surface properties are suitable for loading positively charged or π - π stacked matters like small molecular drugs and small interfering RNA.¹⁶³ Excellent properties of BP nanosheets and the structural changes in thermosensitive hydrogels are useful in achieving the purpose of controlled drug release.^{150,164} In addition, the drug release rate and release amount can also be tuned by changing the water content of hydrogel, the concentration of nanosheets, light intensity, and irradiation time

of the laser.¹⁶⁵ GO nanosheets contain numerous -OH, -CHO, and -COOH groups on their surface, offering massive active sites to bind with biomacromolecules such as protein and nucleic acids.¹⁶⁶ In addition, the Xenes could convert light into heat that further softens and melts drug-loaded platforms.⁴⁸ The drug release rate can also be optimized by laser irradiation duration, laser intensity, the concentration of Xene, and the composition of hydrogels.

Cancer therapy. Photonic therapy (PTT and PDT) is a promising cancer treatment with minimal invasiveness. Xene hydrogels also exhibit

excellent photonic performance and good biodegradability. Research revealed that BP-incorporated hydrogels serve as controlled drug release platforms for PTT.¹⁶⁷ Emetine loading in the BP hydrogel system can weaken tumor resistance to BP-mediated PTT, owing to the near-infrared light-controlled release, thus, inhibiting stress granule formation involved in the resistance process.¹⁴⁹ Qin et al. prepared an injectable thermosensitive hydrogel containing BP nanoparticles loaded with gemcitabine. Under near-infrared (NIR)-laser irradiation, the temperature rise in BP material was induced to achieve the intratumoral controlled release of gemcitabine.¹⁵⁰ Similarly, Li et al. encapsulated BP nanosheets and docetaxel micelles in an injectable thermally reversible hydrogel. By controlling the drug release in the tumor tissue, the drug system showed an exceptional therapeutic effect.⁴⁹ In addition, tumor cell membrane-coated BP quantum dots, together with PD-1 antibody and immunogenic adjuvants, were also embedded in hydrogels to function as a tumor vaccine.⁴² After subcutaneous injection of vaccine hydrogel, the NIR irradiation recruited DC and aided T lymph cell activation, while the immune modulators crippled immune suppression of tumor cells. As a result, the photothermal hydrogel systems activated multi pathways to boost the immune system, realizing the inhibition of tumor recurrence.

Tissue engineering. Tissue engineering is a promising strategy to treat injuries by replacing damaged tissue with manufactured implants.¹⁶⁸ To date, several Xene hydrogels have been used in bone and cardiac tissue engineering. Bone tissue engineering requires materials that promote bone generation and repair.^{169,170–172} Studies indicated that graphene and its derivatives promote osteogenic differentiation by acting as a preconcentration platform for osteogenic inducers due to the aromatic structure and strong noncovalent interactions.^{173–176} Graphene hydrogel films show cell adhesion, spreading, and proliferation, and also stimulated osteogenic differentiation of stem cells after being implanted into subcutaneous sites of rats. The *in vivo* swell and crack of the hydrogel indicate its biocompatibility.¹⁵¹ BP-based hydrogels promote osteogenesis through biomineralization. BP gradually degrades to phosphates, an important constituent of bone, filling injured bone and mineralizing with calcium ions to promote bone generation.¹⁵² Lu et al. fabricated BP and CNT co-loaded hydrogels for bone injury repairment, and the marriage of these materials witnessed better bone tissue engineering effects due to the increased electrical conductivity of the carbon tube under electrical stimulation.¹⁵³

Cardiac cells are non-proliferation cells. Replacing defective cardiac tissue with manufactured hydrogels provides an efficient pathway for severe cardiac injury patients. The contractibility and conductivity of cardiac cells make cardiac tissue engineering very picky about the similar properties of materials,¹⁷⁷ such as graphene hydrogels.^{178,179} Ali Khademhosseini's group constructed several graphene hydrogels for connecting cardiac tissues. They designed an anionic plasmids-loaded GO hydrogel for acute myocardial infarction treatment. The loaded DNA efficiently transfected damaged cardiac tissues, and the soft nature of hydrogel reduced the injury of injected materials.¹⁵⁴ Another example was methacryloyl-substituted recombinant human tropoelastin (MeTro)/GO hybrid hydrogel. GO served as the hydrogel network connector under compression. The addition

Table 1. The comparisons between different Xene materials

| Periodic group | Element | 2D form | Stability | Tunable band gap | Photothermal conversion efficiency (%) | Catalytic ability | Electrical property |
|----------------|---------|-------------|--|--|--|--|--|
| IIIA | B | borophene | Highly chemical stable, photostable ³⁰ | Zero or near-zero bandgap, ⁷⁸ opened by hydrogenation/ fluorination or a shear strain (in theoretical calculations) ⁷⁹ | 42.50% ³⁰ | Hydrogen evolution; ⁸⁰ oxygen reduction; oxygen evolution; CO ₂ electroreduction ⁷⁹ | High electrical conductivity (in theoretical calculations) ^{81,82} |
| IIIA | Ga | gallenene | stable ⁸³ | zero or near-zero bandgap ⁷⁸ | no report | no report | metallic, ⁸⁴ superconductivity ⁸⁵ |
| IVA | C | graphene | aggregating in saline ⁸⁶ | zero or near-zero bandgap ⁷⁸ | 49.13% (single-layered graphene); 46.26% (GO) ⁸⁷ | nitrobenzene hydrogenation (GO); ⁸⁸ oxidation of sulfides, olefins and various hydrocarbons (GO) ⁸⁹ | high electrical conductivity (in theoretical calculations) ⁷⁸ |
| IVA | Si | silicene | biodegradable ⁹⁰ | zero or near-zero bandgap; ⁷⁸ opened under vertical electric field (in theoretical calculations) ⁹¹ | 36.09% ⁹⁰ | CO ₂ hydrogenation; ⁹² nitrobenzene reduction ⁹³ (in theoretical calculations) | resistance: 224~823Ω under different conditions ⁹⁴ ; high electrical conductivity ⁷⁸ |
| IVA | Ge | germanene | rapid degradation ^{95,96} | opened under vertical electric field (in theoretical calculations) ⁹¹ | 38.40% ⁹⁵ | picric acid violet light-assisted photodegradation (hydrogenated germanene) ⁹⁷ | semiconducting (in theoretical calculations); ⁹⁸ from insulator to metal after heating ⁹⁹ |
| IVA | Sn | stanene | aggregating in saline ¹⁰⁰ | tuned under vertical electric field (in theoretical calculations) ¹⁰¹ | 48.60% ¹⁰⁰ | CO ₂ reduction (in theoretical calculations) ¹⁰² | semiconducting (in theoretical calculations) ¹⁰³ |
| VA | P | phosphorene | biodegradable (black) ²⁵ | layer-dependent band gap ⁷⁸ | 19.8 °C increased after irradiation (BPQD, 10 ppm, 10 min, 1 W cm ⁻²) ¹⁰⁴ | oxygen evolution; ^{105,106} ¹ O ₂ generation; ¹⁰⁷ ·OH and ·O ₂ ⁻ generation ¹⁰⁸ | semiconducting (in theoretical calculations) ¹⁰⁹ |
| VA | As | arsenene | biodegradable ¹¹⁰ | layer-dependent band gap (in theoretical calculations) ¹¹¹ | 14 °C increased after irradiation (100 μg/mL, 5 min, 2 W cm ⁻²) ¹¹⁰ | Chlorine evolution ¹¹² | Semiconducting (in theoretical calculations) ¹¹³ |
| VA | Sb | antimonene | Highly stable in the atmosphere ^{114,115} | layer-dependent band gap (in theoretical calculations) ¹¹¹ | 44.60% ¹¹⁶ | Ammonia synthesis under ambient conditions (oxidized antimonene) ¹¹⁷ | Semiconducting (in theoretical calculations) ¹¹⁸ |
| VA | Bi | bismuthene | Biodegradable ¹¹⁹ | Shrank with nerve agents assimilated on the surface ¹²⁰ | 21.3% ¹¹⁹ | CO ₂ reduction; ¹²¹ CO generation ¹¹⁹ | Semiconducting: electronic conductivity reached up to 10 ⁸ S m ⁻¹ (in theoretical calculations) ¹²² |
| VIA | Se | selenene | biodegradable ¹²³ | no report | no report | no report | semiconducting (in theoretical calculations) ¹²⁴ |
| VIA | Te | tellurene | biodegradable ¹²⁵ | layer-dependent band gap (in theoretical calculations) ¹²⁶ | 55% ¹²⁵ | no report | semiconducting ⁷⁸ |

Table 2. The applications of Xene hydrogels

| Field | Application | Xene | Polymer/Other Linker | |
|-------------|----------------------------|----------------------------|---|----------------------------|
| Biomedical | Cancer therapy | BP nanosheets | Low-melting-point agarose ¹⁴⁹ Pluronic F-127 ¹⁵⁰ Pluronic F-127 and hyaluronic acid ⁴² | |
| | Bone regeneration | graphene | no polymer ¹⁵¹ | |
| | Bone regeneration | BP nanosheets | Gelatin methacrylate and U-Arg-PEA ¹⁵² oligo(poly(ethylene glycol) fumarate) ¹⁵³ | |
| | Cardiac tissue engineering | graphene | low methacrylated gelatin methacrylate ¹⁵⁴ methacryloyl-substituted tropoelastin ¹⁵⁵ | |
| | Neural differentiation | BP nanosheets | gelatin methacryloyl ⁴¹ | |
| | Wound healing | BP nanosheets | fibrin ¹⁵⁶ | |
| | Wound healing | antimonene | chitosan ¹⁴² | |
| Sensing | Biosensor | graphene | L-cysteine ¹⁵⁷ | |
| | Energy | Battery | graphene and BP nanosheets | no polymer ⁶⁵ |
| | | Battery | graphene | no polymer ^{46,v} |
| Environment | Supercapacitor | graphene | polyaniline ¹⁵⁸ | |
| | Hydrogen production | graphene | no polymer ¹⁵⁹ | |
| | Water purification | BP nanosheets | chitosan ⁴³ | |
| | Water purification | graphene and BP nanosheets | no polymer ¹⁶⁰ | |

of GO enhanced the torsion tolerance and conductivity of protein hybrid hydrogels.¹⁵⁵

The conductivity of Xene hydrogel (GelMA-BP@PDA) is also applied for neural-like cell differentiation from mesenchymal stem cells under electrical stimulation.⁴¹ The immunofluorescent staining revealed an increased level of neuronal-specific marker β -Tubulin III (Tuj1) and MAP2 of GelMA-BP@PDA, compared with the GelMA hydrogels under electrical stimulation, and a slight decrease in glial marker GFAP content.

Wound healing. The sprayed gel can cover the wound tissue in a large area, and Xene incorporation can promote wound repair. Therefore, an intelligent BP-based gel was developed by our group with rapid formation and NIR response to solve chronic diabetic ulcers.¹⁵⁶ Figures 6A–6C show that the *in situ* sprayed BP-based gel can act as a temporary bionic "skin," accelerating the healing of chronic wounds by promoting endothelial cell proliferation, and angiogenesis, temporarily shielding tissue from contact with the external environment. In addition, the hydrogel is also used as a drug "repository" to store bactericidal BP and painkiller lidocaine hydrochloride (Lid). Similarly, Wang et al. incorporated AM NSs into the chitosan network structure to fabricate a chitosan/AM NSs hydrogel composite, in a first attempt to apply AM NSs in the antibacterial field. The hybrid hydrogel collected bacteria through electrostatic interaction of chitosan with their cell membrane and eliminated them by outstanding photothermal effect of AM NSs. During the *in vitro* experiment, the AM-based hydrogel demonstrated a broad-spectrum antibacterial property against *E. coli* (97.1%) and *S. aureus* (100%).¹⁴²

The sprayed Xene hydrogel can induce rapid gelation to form a gelled membrane on tumor resection wounds under a rapid photo-induced sol-gel transition upon photoirradiation. Complications such as the infection occurring after surgery can be addressed by Xene hydrogels owing to the good photonic antibacterial performance of the proposed synthesized membrane. Furthermore, germanene hydrogels can serve as post-surgical treatment agents to prevent tumor recurrence and avoid wound infection.²⁷

Sensors

The biosensor is a device consisting of an identification and signal conversion element, responding to target variations (e.g., concentration changes of materials), with high selectivity and analytical sensitivity.^{180–184} The basis for Xene hydrogels as sensors originates from the optical/electrical performance and their

modifiable surface, stimuli responsiveness of hydrogels, and their adsorption capacity.^{185–187} In other words: (1) the Xene and hydrogel can capture targeting materials via several interactions; (2) the stimulus-sensitive hydrogels can change the gelatinous state with the external environment; and (3) Xenes can improve the sensitivity and reaction time of hydrogel biosensors due to abundant sp² bonds and increased electrochemical reactivity and mass transfer of electrons. Singh et al. fabricated a dual-modality microfluidic biosensor based on graphene-based hydrogel to quantify human cardiac myoglobin (cMb) (Figure 6D).¹⁵⁷ They used reduced GO with an L-cysteine amino acid to connect the cMb antibody via covalent interactions (-COOH on cysteine and -NH₂ on antibody), as shown in Figures 7E–7G. The CV responses of RGO, Cys, and Cys-RGO hydrogel electrodes and cMAB/Cys-RGO bioelectrode indicated that Cys-RGO hydrogels offered a larger porous surface and higher electron transfer rate than Cys alone, thus improving the biosensor efficiency. Differential pulse voltammetry responses were measured by a microfluidic chip (CMAB/Cys/Au) without RGO hydrogel and different concentrations of standard cMb were introduced. The response peak current decreased with the increase in cMb concentration, indicating the effectiveness of the designed sensor.

Energy storage and production

In recent years, the construction of efficient energy storage devices has gained tremendous attention due to the increasing industrialization and growing population.¹⁸⁸ Among them, supercapacitor with excellent energy storage capacity and power density has been highly demanded, which stores energy either by surface adsorption of electrolytic ions or fast surface redox reactions.¹⁸⁹ Xenes exhibit exceptional properties as electrode materials.¹⁸⁹ For example, Mei et al. prepared an interesting BPNs@TiO₂@G hydrogel with an exceptional 2D-TiO₂-2D structure. Compared with traditional hydrogels, this 2D-TiO₂-2D structure exhibits outstanding high specific surface area, abundant hierarchical porous, and excellent conductivity to store and release Li ions during charging and discharging. High discharge capacity significantly improved cyclic capacity and superior rate capacity. Such a BPNs@TiO₂@G hydrogel provides a valuable research direction for the development of other metal oxide nanomaterials with efficient energy storage, inspired by the interfacial chemistry of energy storage materials (Figures 7A–8C).⁶⁵ This team also successfully fabricated a highly phosphorus-doped 3D graphene hydrogel through a simple one-step hydrothermal process to achieve increased Li-ion storage.⁴⁶ Extremely high amounts of

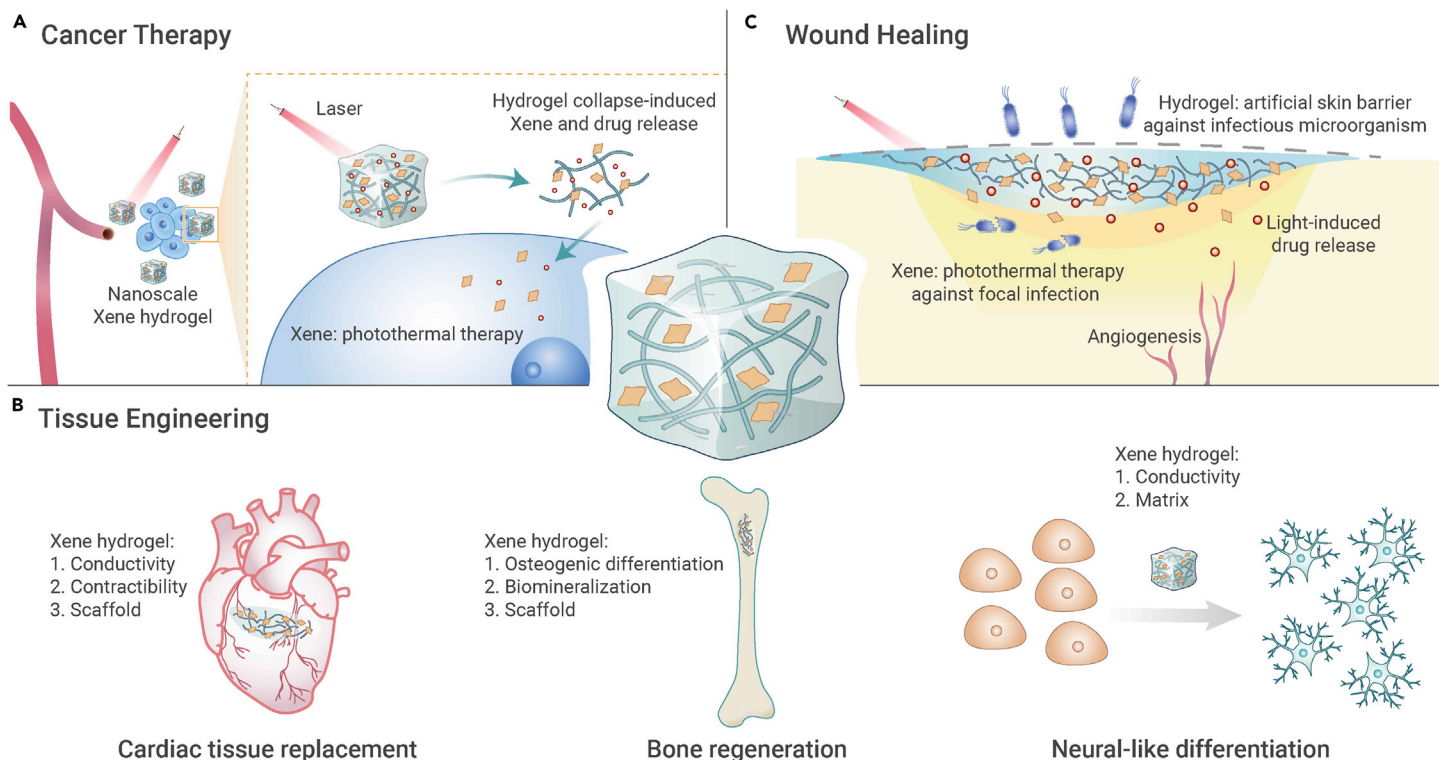


Figure 5. Medical applications of Xene hydrogels (A) Loaded with therapeutic drugs, nanoscale Xene hydrogel can be delivered to the tumor site and be decomposed in tumor cells upon light irradiation to release the cargos. Xenes can function as photothermal agents against cancer cells. (B) Xene hydrogel can be utilized in cardiac tissue replacement, bone generation, and neural-like differentiation. (C) Xene hydrogel can be applied to protect wounds from infectious microorganisms. Similar to the case in the tumor site, Xene can convert light energy into heat to kill focal bacteria. Also, released cargos can exert different functions such as promoting angiogenesis.

phosphorus (even up to 4.84%) and various sizes of apertures (ranging from 1.7 to 17.5 nm) were used in phosphorus-doped 3D graphene hydrogel for construction of heterostructured 2D BP on graphene. Therefore, Li-ion storage performance was further boosted by abundant and stable C-P bonds, significantly shortening the circulation time and are convenient to obtain and lose Li-ion. This is a potential strategy for the future development of phosphorus-doped hydrogel networks while avoiding using highly toxic organophosphates.

Moreover, the conductive and stretchable properties of the hydrogel make it particularly suitable for flexible electronic materials. Xiao et al reported a 3D polyaniline/graphene hydrogel-based conceptual all-gel-state fibrous supercapacitor with excellent plasticity and electrochemical properties. The supercapacitor is designed through the self-assembly of GO and carbon nanotube macromolecular structure (Figure 7D).¹⁵⁸ Due to the strong macromolecular interaction between carbon fiber and graphene, the 3D hybrid hydrogel exhibited uniform connectivity and enhanced mechanical properties, thereby greatly reducing aggregation during fiber formation. In addition, a large strain (up to 40%) was achieved and the volumetric energy density reached up to 8.80 mWh cm^{-3} at a power density of 30.77 mW cm^{-2} .

Solar photocatalytic hydrolysis is an important way to alleviate energy and environmental pressure to produce hydrogen. Ho et al. prepared graphene and TiO_2 hybrid NGH hydrogel to produce hydrogen under light.¹⁵⁹ In the absence or presence of UV-visible, 3D NGH, and NGH-Au generated hydrogen more efficiently than 1D or 2D TiO_2 and RGO- TiO_2 , attributed to the 3D hydrogel structure, which is more conducive to charge quick separation.

Water purification

The water purification by Xene hydrogels mainly includes two steps: pollutant capture and disposal. The pollutants such as bacteria, organics, and inorganic particles are adsorbed in hydrogel pores or on the Xene's surface and subsequently sterilized or decomposed via the enhanced functional Xene.^{190–194} Compared with traditional physical (UV, heat sterilization by size exclusion, etc.) and chemical methods (chlorine, ozone, and metal ion), Xene hydrogels are less toxic to human health, have low energy consumption, and generate less environmental pollution and global warming.^{195,196} Li et al. constructed a sandwich-like water disinfection system (CSBPP) based on chitosan hydrogel, BP

nanosheets, and layer-by-layer stacking of chitosan hydrogel (Figure 8A). At an appropriate concentration of glutaraldehyde, the removal efficiency of bacteria reached 98%, as shown in Figure 8B. At the same time, BP nanosheets showed excellent photothermal conversion efficiency under NIR radiation, enhancing the CSBPP's ability to kill bacterial cells adsorbed on hydrogel scaffolds through the photothermal effect (Figure 8C). CSBPP circumvented membrane fouling caused by undesirable bacterial growth and was more environmentally benign, revealing an overall potential for potent, sustained, and safe water disinfection.⁴³

Many researchers developed highly reusable and superhydrophobic aerogels or hydrogels for photocatalysts to eliminate water waste and air pollutants.^{197–199} For sewage treatment, Wang et al. prepared RGO-BP-Pd composite hydrogel using rGO as a catalyst carrier (Figure 8D). The prepared hydrogels showed good catalytic performance for 4-nitrophenol. Specifically, with the participation of RGO-Pd-based composite hydrogels, NaBH_4 provided negative hydrogen ions to attack 4-nitrophenol and reduce 4-nitrophenol to less toxic 4-aminophenol (Figure 8E). The reasons for the high efficiency of the catalytic system are revealed in Figure 8F. Due to favorable band structure, the photoexcited electrons in the conduction band of BP NS were transferred to the conduction band of Pd. Moreover, the hole in the valence band of PdNPs was transferred to the valence band of BP NS. Since the electron-hole pairs in BP NS and Pd were relatively independent, the charge carriers exhibited a long lifetime.¹⁶⁰

CONCLUSIONS AND FUTURE OUTLOOK

Various Xene hydrogels have rapidly emerged in recent years with significant advantages over many other static platforms, establishing new standards for the development of complex and powerful platforms. Tremendous design flexibilities and unique opportunities for soft devices have benefited from the combination of Xenes and hydrogels, and the gain-of-function has enabled those devices with exotic features and augmented application performance. In this review, Xene hydrogels have been discussed in detail, especially the synthesis methods, properties, and applications. The general characteristics, advantages, and disadvantages of each synthesis method are summarized for readers to choose a suitable method according to different needs. Then the general and special properties of hydrogels and emerging Xenes are introduced in detail and compared with traditional hydrogels to illustrate their advantages and challenges.

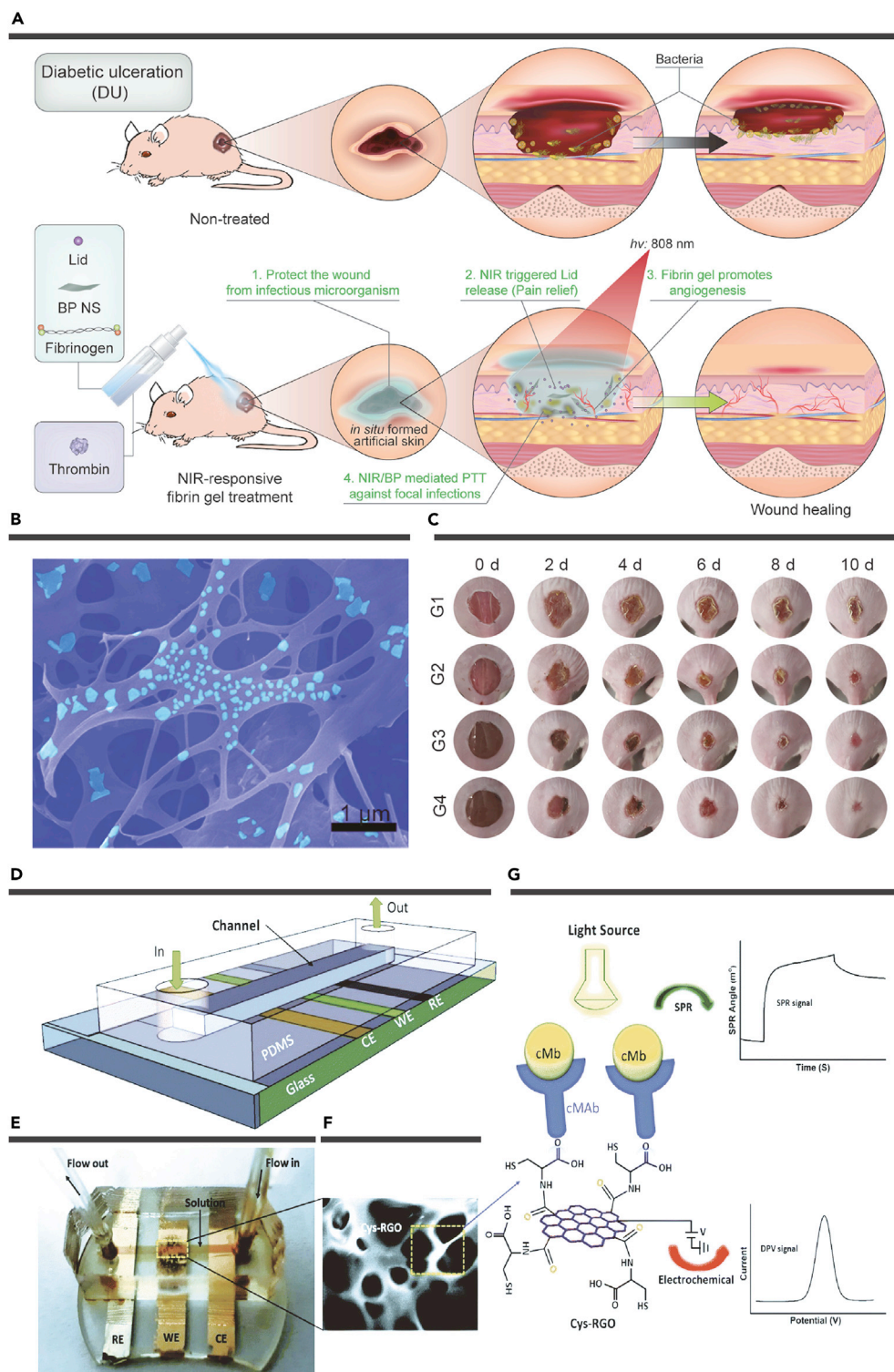


Figure 6. Application of Xene hydrogel in biomedicine and biosensor (A) Scheme of *in situ* sprayed BP gel for accelerated wound healing in diabetic ulceration. (B) Pseudocolor scanning electron microscopy (SEM) image of BP@Gel. (C) Images of wound healing in mice skin at different times after different treatments: G1, control; G2, Gel; G3, BP@Gel; and G4, BP@Gel@Lid + NIR.¹⁵⁶ (D) Schematic illustration of the incorporated dual-modality Cys-RGO hydrogel microfluidic biosensor chip for the detection of cMb. (E) A photograph of the nanoengineered integrated dual-modality mesoporous Cys-RGO hydrogel microfluidic biosensor chip. (F) SEM image of the integrated Cys-RGO hydrogel. (G) Incorporated dual-modality Cys-RGO hydrogel sensor mechanism revealing the coupling of light and voltage sources to measure electrochemical and SPR signals¹⁵⁷ (copyright Proceedings of the National Academy of Sciences of the United States of America, 2020; copyright Royal Society of Chemistry, 2020).

gregation of skeletal muscle fiber bundles are vital to their related functions.^{203–205} However, most of the existing Xene-based hydrogels have uniform Xene distribution and disordered structure, hindering their anisotropic mechanical properties and functions. Therefore, the development of highly ordered Xene-based hydrogels can achieve anisotropic mechanical, optical, and biological properties, further promoting the development of Xene-based hydrogels in bioengineering applications. Also, the research on theory and mechanism will provide great guidance for the rational design of Xene hydrogels.

The interaction between additives and macromolecules can provide another direction for the development of anisotropic materials. For example, γ -glycine can self-assemble between two PVA films via hydrogen bonding (O atoms of glycine and -OH of PVA chain). The sandwiched thin film is heterostructured and piezoelectric, beneficial for biomechanical energy (such as leg stretching).²⁰⁶ Similarly, Xenes can be orderly added into hydrogels to form heterogeneous materials since 2D materials with π bonds and controlled surface chemical modification can react with multitudinous hydrogel polymers.

Also, the Xene distribution can be regulated by external factors. Anisotropic materials are easier to self-align in the desired orientations where the dielectrically/magnetically susceptible axis is parallel to the external, uniform, and static field.²⁰⁷ For example, exploiting the intrinsic anisotropic and magnetic susceptibility of carbon nanotubes is conducive to developing anisotropically luminescent hydrogels via an external magnetic field.²⁰⁸ Organic polar nanocrystals are effectively polarized and orientated in polymer matrices by applying a direct-current electric field, functioning as an electro-optic material for fast and high-capacity optical information processing.²⁰⁹ Therefore, Xene nanosheets with intrinsic anisotropy can be aligned by external electric or magnetic fields.²¹⁰ Mechanical strain changes the alignment of additives with a load transfer medium, i.e., the polymer can also increase the ductility for large plastic deformation.²¹¹ Moreover, stretching polymers can direct them into anisotropic hydrogels due to the maximum crosslinking. Moreover, the Xene distribution can be regulated by external factors as well. Anisotropic materials can be self-aligned in specific orientations with dielectrically/magnetically susceptible axis parallel to the external, uniform, and static field.²⁰⁷ For example, exploiting

Finally, the applications of Xene hydrogels are explored in biomedicine, pollution prevention, and electronic equipment. Our insights on the challenges and future directions of Xene hydrogel in other potential applications are also expressed.

Preparing anisotropic hydrogels

Highly ordered Xene-based hydrogels are a new direction in the area of hydrogel bioengineering.²⁰⁰ In the human body, different tissues such as blood vessels, cornea, and cartilage are natural hydrogels.^{201,202} They are composed of a variety of cells and proteins arranged in an orderly manner, essential to achieve corresponding biological functions. For example, the ordered layered structure of the cornea and the directional ag-

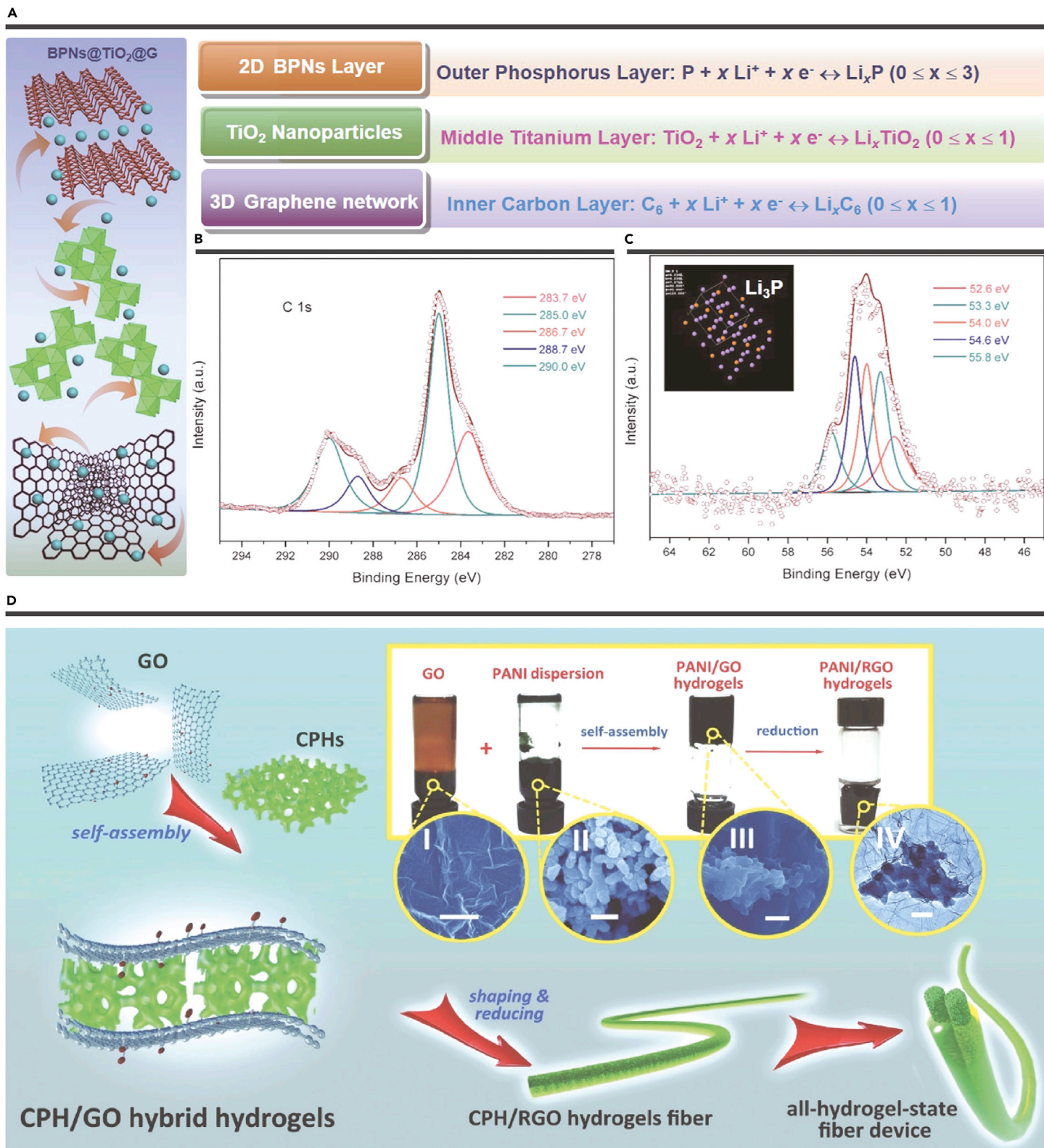


Figure 7. Lithium storage mechanism of 2D-TiO₂-2D heterostructured electrode and PANI/GO hybrid hydrogels formation, shaping/reduction process, and their conductivity (A) Schematic illustration on possible diffusion and transfer paths of Li⁺ ions in BPNs@TiO₂@G composite electrode, (B) C 1s and (C) Li 1s spectra of BPNs@TiO₂@G electrode after cycles. Inset in (C) shows the crystal structures of Li₃P.⁶⁵ (D) Schematic illustration of PANI/GO hybrid hydrogels formation and the reduction of PANI/RGO (the inset) as well as the corresponding SEM and TEM images of samples after freeze-drying¹⁵⁸ (copyright Elsevier, 2019; copyright John Wiley and Sons, 2018.)

the intrinsic anisotropic magnetic susceptibility of carbon nanotubes can develop anisotropically luminescent hydrogels via an external magnetic field.²⁰⁸ Organic polar nanocrystals can be effectively polarized and orientated in polymer matrices under a direct-current electric field, functioning as an electro-optic material for fast and high-capacity optical information processing.²⁰⁹ Therefore,

Xene nanosheets with intrinsic anisotropy exhibit great alignment potential under external electric or magnetic fields.²¹⁰ Mechanical strain can also change the alignment of additives under a load transfer medium, i.e., the polymer can increase the ductility for large plastic deformation.²¹¹ Stretching polymers can produce anisotropic hydrogels due to maximum crosslinking.^{212,213}

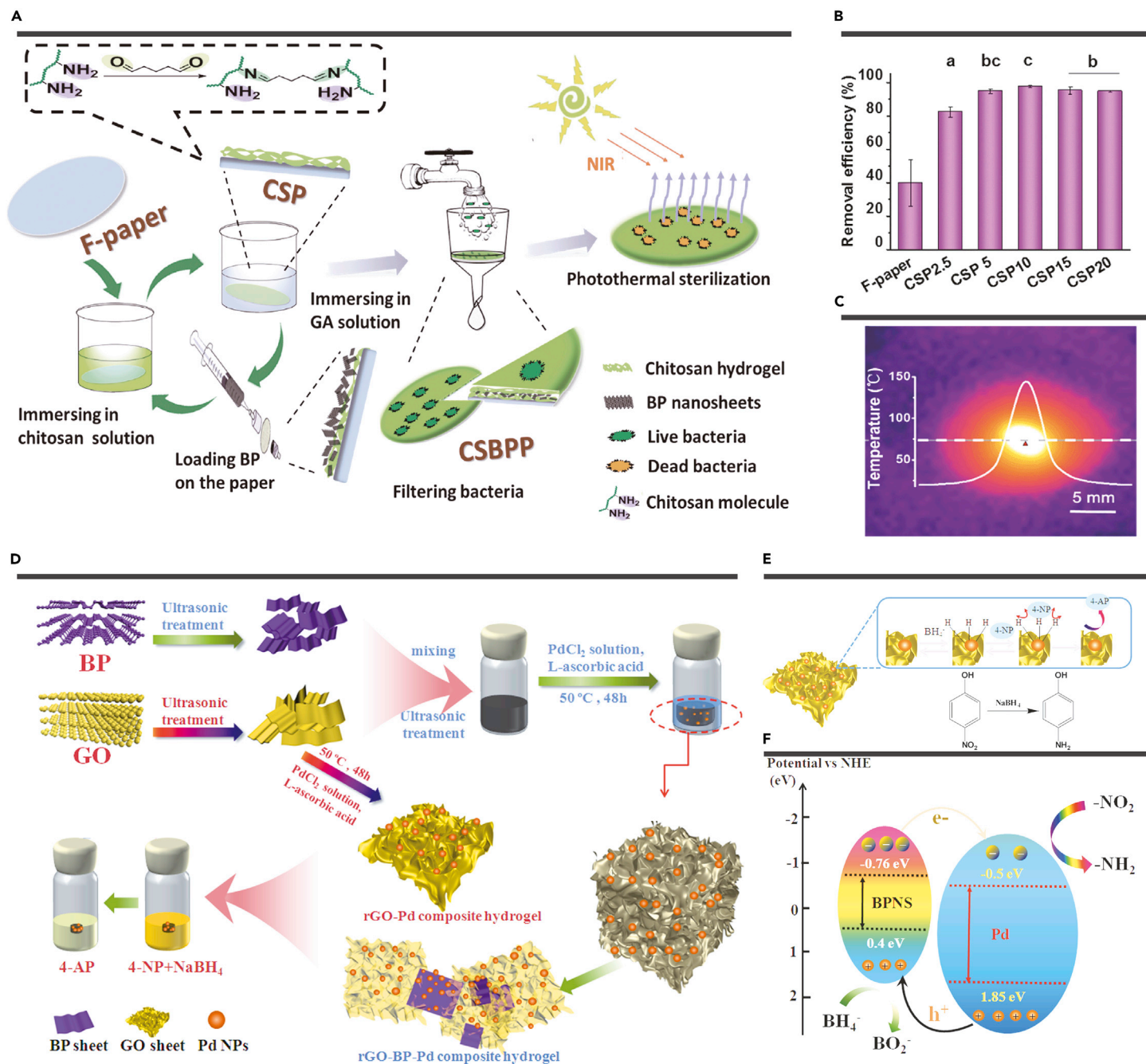


Figure 8. Application of Xene hydrogel in water treatment (A) Fabrication process of the sandwich-structured filter systems and the description of bacteria removal–disinfection. (B) Removal efficiency for *E. coli* treated with the F-paper and CSP with different crosslinking degrees.⁴³ (C) Thermographic image of CSBPP4 after 10 min of NIR illumination. (D) Schematic illustration of the synthesis process and catalytic performances of the prepared rGO-based composite hydrogels. (E) Schematic of the Langmuir-Hinshelwood model and (F) the catalytic mechanism for 4-NP catalytic reduction¹⁶⁰ (copyright Elsevier, 2020; copyright Royal Society of Chemistry, 2019).

Developing artificial skin

Artificial skin first appeared in skin wound healing with promising efficiency as protective, soft, stretchable, water-rich, and self-healable characteristics.²¹⁴ Hydrogels with appropriate mechanical properties (e.g., 0.5–1.95 MPa of Young's moduli, 140%–180% of ductility, and over 70% of water content) have also been listed as potential candidates.²¹⁵ Nowadays, artificial skins are more like electronic sensors. Similar to real skin, delivering surrounding variables to the nervous system, the artificial skin always converts mechanical stress or temperature into electrical signals.²¹⁶ Xene is the icing on the cake in this field,²¹⁶ due to the perfect mechanical properties of hydrogels and increased conductivity, as mentioned above. More importantly, some Xenes are piezoelectric and even pyroelectric, such as BP, imparting outstanding sensing performances to the artificial skin. In addition, the Xene hydrogel-based artificial skin is more sensitive than the ZnO-based skins due to the plane structure, more active sites, and larger electron cloud density.²¹⁷ Related research proved that the photocatalytic

performance of additives can change the inner structure and electronic conductivity of hydrogels.²¹⁸ Xene hydrogel-based artificial skin can increase the antibacterial ability also under external environments by producing reactive oxygen species.²¹⁹

Clinical translation of *in vivo* applications

Xene hydrogels can be applied *in vivo* via surgical implantation, local injection, or systemic administration. The priority is safety and biocompatibility. Most hydrogels are biocompatible; however, the metabolism of Xenes has not been fully understood yet. Figuring out the interactions between the body and Xenes is conducive to exploring more *in vivo* applications. Stability is another key point to be taken into consideration. Surgical implants (such as tissue scaffolds) always work for a long time and require long-term structure and function stability. In this case, degradable BP is not an ideal choice. However, due to the injectability of most hydrogels, they can be used as drug reservoirs and controlled drug

release, and the type and amount of Xenics should promise the injectability of hydrogels. Although Xenics-based nanogel can be developed for intravenous injection, the systemic side effects cannot be ignored. Despite this, Xenics hydrogels have significant clinical transformation value due to the combined effect of the two components.

REFERENCES

- Zhang, Y.S., and Khademhosseini, A. (2017). Advances in engineering hydrogels. *Science* **356**, eaaf3627.
- Chen, W., and Tao, W. (2022). Precise control of the structure of synthetic hydrogel networks for precision medicine applications. *Matter* **5**, 18–19.
- Ouyang, J., Chen, W., and Tao, W. (2022). Design of application-optimized hydrogels based on a swollen polymer network model. *Matter* **5**, 2471–2473.
- Liu, X., Liu, J., Lin, S., and Zhao, X. (2020). Hydrogel machines. *Mater. Today* **36**, 102–124.
- Peng, N., Wang, Y., Ye, Q., et al. (2016). Biocompatible cellulose-based superabsorbent hydrogels with antimicrobial activity. *Carbohydr. Polym.* **137**, 59–64. <https://doi.org/10.1016/j.carbpol.2015.10.057>.
- Edwards, J., and Stapley, S. (2010). Debridement of diabetic foot ulcers. *Cochrane Database Syst. Rev.* **1**, CD003556.
- Caccavo, D., Cascone, S., Lamberti, G., and Barba, A.A. (2018). Hydrogels: experimental characterization and mathematical modelling of their mechanical and diffusive behaviour. *Chem. Soc. Rev.* **47**, 2357–2373.
- Calvert, P. (2009). Hydrogels for soft machines. *Adv. Mater.* **21**, 743–756.
- Noor, N., Shapira, A., Edri, R., et al. (2019). 3D Printing of personalized thick and perfusable cardiac patches and hearts. *Adv. Sci.* **6**, 1900344.
- Zisch, A.H., Schenk, U., Schense, J.C., et al. (2001). Covalently conjugated VEGF–fibrin matrices for endothelialization. *J. Control. Release* **72**, 101–113.
- Rafat, M., Li, F., Fagerholm, P., et al. (2008). PEG-stabilized carbodiimide crosslinked collagen-chitosan hydrogels for corneal tissue engineering. *Biomaterials* **29**, 3960–3972.
- Bhattacharya, M., Malinen, M.M., Lauren, P., et al. (2012). Nanofibrillar cellulose hydrogel promotes three-dimensional liver cell culture. *J. Control. Release* **164**, 291–298.
- Li, J., and Mooney, D.J. (2016). Designing hydrogels for controlled drug delivery. *Nat. Rev. Mater.* **1**, 16071.
- Van Vlierberghe, S., Dubruel, P., and Schacht, E. (2011). Biopolymer-based hydrogels as scaffolds for tissue engineering applications: a review. *Biomacromolecules* **12**, 1387–1408.
- Hoffman, A.S. (2002). Hydrogels for biomedical applications. *Adv. Drug Deliv. Rev.* **54**, 3–12.
- Lee, K.Y., and Mooney, D.J. (2001). Hydrogels for tissue engineering. *Chem. Rev.* **101**, 1869–1879.
- Hamidi, M., Azadi, A., and Rafiei, P. (2008). Hydrogel nanoparticles in drug delivery. *Adv. Drug Deliv. Rev.* **60**, 1638–1649.
- Pan, S., Li, J., Wen, Z., et al. (2021). Halide perovskite materials for photo(electro)chemical applications: dimensionality, heterojunction, and performance. *Adv. Energy Mater.* **12**, 2004002.
- Tang, W., Teng, K., Guo, W., et al. (2022). Defect-engineered Co₃O₄@nitrogen-deficient graphitic carbon nitride as an efficient bifunctional electrocatalyst for high-performance metal-air batteries. *Small* **18**, e2202194.
- Zhong, M., Xia, Q., Pan, L., et al. (2018). Thickness-dependent carrier transport characteristics of a new 2D elemental semiconductor: black arsenic. *Adv. Funct. Mater.* **28**, 1802581.
- Hu, Y., Wang, X., Qi, Z., et al. (2021). Wet chemistry vitrification and metal-to-semiconductor transition of 2D gray arsenene nanoflakes. *Adv. Funct. Mater.* **31**, 2106529.
- Mannix, A.J., Kiraly, B., Hersam, M.C., and Guisinger, N.P. (2017). Synthesis and chemistry of elemental 2D materials. *Nat. Rev. Chem.* **1**, 0014.
- Tsang, V.L., and Bhatia, S.N. (2004). Three-dimensional tissue fabrication. *Adv. Drug Deliv. Rev.* **56**, 1635–1647.
- Mandrycky, C., Wang, Z., Kim, K., and Kim, D.H. (2016). 3D bioprinting for engineering complex tissues. *Biotechnol. Adv.* **34**, 422–434.
- Tao, W., Zhu, X., Yu, X., et al. (2017). Black phosphorus nanosheets as a robust delivery platform for cancer therapeutics. *Adv. Mater.* **29**, 1603276.
- Wang, X., Hu, Y., Mo, J., et al. (2020). Arsenene: a potential therapeutic agent for acute promyelocytic leukaemia cells by acting on nuclear proteins. *Angew. Chem. Int. Ed. Engl.* **59**, 5151–5158.
- Feng, C., Ouyang, J., Tang, Z., et al. (2020). Germanene-based theranostic materials for surgical adjuvant treatment: inhibiting tumor recurrence and wound infection. *Matter* **3**, 127–144.
- Zhang, L., Liang, J., Huang, Y., et al. (2009). Size-controlled synthesis of graphene oxide sheets on a large scale using chemical exfoliation. *Carbon* **47**, 3365–3368.
- Chen, Y., Chen, C., Kealhofer, R., et al. (2018). Black arsenic: a layered semiconductor with extreme in-plane anisotropy. *Adv. Mater.* **30**, e1800754.
- Ji, X., Kong, N., Wang, J., et al. (2018). A novel top-down synthesis of ultrathin 2D boron nanosheets for multimodal imaging-guided cancer therapy. *Adv. Mater.* **30**, e1803031.
- Niu, T., Zhou, W., Zhou, D., et al. (2019). Modulating epitaxial atomic structure of antimonene through interface design. *Adv. Mater.* **31**, e1902606.
- Feng, B., Zhang, J., Zhong, Q., et al. (2016). Experimental realization of two-dimensional boron sheets. *Nat. Chem.* **8**, 563–568.
- Zhu, F.F., Chen, W.J., Xu, Y., et al. (2015). Epitaxial growth of two-dimensional stanene. *Nat. Mater.* **14**, 1020–1025.
- Shao, Y., Liu, Z.L., Cheng, C., et al. (2018). Epitaxial growth of flat antimonene monolayer: a new honeycomb analogue of graphene. *Nano Lett.* **18**, 2133–2139.
- Chen, Z., Lv, Z., Zhang, Z., et al. (2021). Advanced microfluidic devices for fabricating multi-structural hydrogel microspheres. *Exploration* **1**, 20210036.
- Bashir, S., Hina, M., Iqbal, J., et al. (2020). Fundamental concepts of hydrogels: synthesis, properties, and their applications. *Polymers* **12**, 2702.
- Leng, F., Zheng, M., and Xu, C. (2021). 3D-printed microneedles with open groove channels for liquid extraction. *Exploration* **1**, 20210109.
- Ji, Y., Ghosh, K., Shu, X.Z., et al. (2006). Electrospun three-dimensional hyaluronic acid nanofibrous scaffolds. *Biomaterials* **27**, 3782–3792.
- Malda, J., Visser, J., Melchels, F.P., et al. (2013). 25th anniversary article: engineering hydrogels for biofabrication. *Adv. Mater.* **25**, 5011–5028.
- Zhang, F., Li, Y.H., Li, J.Y., et al. (2019). 3D graphene-based gel photocatalysts for environmental pollutants degradation. *Environ. Pollut.* **253**, 365–376.
- Xu, C., Xu, Y., Yang, M., et al. (2020). Black-phosphorus-incorporated hydrogel as a conductive and biodegradable platform for enhancement of the neural differentiation of mesenchymal stem cells. *Adv. Funct. Mater.* **30**, 2000177.
- Ye, X., Liang, X., Chen, Q., et al. (2019). Surgical tumor-derived personalized photothermal vaccine formulation for cancer immunotherapy. *ACS Nano* **13**, 2956–2968.
- Li, D., Zhao, Q., Zhang, S., et al. (2019). Filtration-based water treatment system embedded with black phosphorus for NIR-triggered disinfection. *Environ. Sci. Nano* **6**, 2977–2985.
- Bhattacharya, S., and Samanta, S.K. (2016). Soft-nanocomposites of nanoparticles and nanocarbons with supramolecular and polymer gels and their applications. *Chem. Rev.* **116**, 11967–12028.
- Liang, J., Huang, Y., Zhang, L., et al. (2009). Molecular-level dispersion of graphene into poly(vinyl alcohol) and effective reinforcement of their nanocomposites. *Adv. Funct. Mater.* **19**, 2297–2302.
- Mei, J., He, T., Zhang, Q., et al. (2020). Carbon-phosphorus bonds-enriched 3D graphene by self-sacrificing black phosphorus nanosheets for elevating capacitive lithium storage. *ACS Appl. Mater. Interfaces* **12**, 21720–21729.
- Peng, X., He, C., Liu, J., and Wang, H. (2016). Biomimetic jellyfish-like PVA/graphene oxide nanocomposite hydrogels with anisotropic and pH-responsive mechanical properties. *J. Mater. Sci.* **51**, 5901–5911.
- Yang, G., Wan, X., Gu, Z., et al. (2018). Near infrared photothermal-responsive poly(vinyl alcohol)/black phosphorus composite hydrogels with excellent on-demand drug release capacity. *J. Mater. Chem. B* **6**, 1622–1632.
- Li, R., Shan, L., Yao, Y., et al. (2021). Black phosphorus nanosheets and docetaxel micelles co-incorporated thermoreversible hydrogel for combination chemo-photodynamic therapy. *Drug Deliv. Transl. Res.* **11**, 1133–1143.
- Liu, R., Liang, S., Tang, X.-Z., et al. (2012). Tough and highly stretchable graphene oxide/polyacrylamide nanocomposite hydrogels. *J. Mater. Chem.* **22**, 14160–14167.
- Xing, C., Chen, S., Qiu, M., et al. (2018). Conceptually novel black phosphorus/cellulose hydrogels as promising photothermal agents for effective cancer therapy. *Adv. Healthc. Mater.* **7**, e1701510.
- Shao, J., Ruan, C., Xie, H., et al. (2018). Black-phosphorus-incorporated hydrogel as a sprayable and biodegradable photothermal platform for postsurgical treatment of cancer. *Adv. Sci.* **5**, 1700848.
- Zhu, C.-H., Lu, Y., Peng, J., et al. (2012). Photothermally sensitive poly(N-isopropylacrylamide)/graphene oxide nanocomposite hydrogels as remote light-controlled liquid microvalves. *Adv. Funct. Mater.* **22**, 4017–4022.
- Wu, R.S., Lin, J., Xing, Y.M., et al. (2019). pH-sensitive black phosphorus-incorporated hydrogel as novel implant for cancer treatment. *J. Pharm. Sci.* **108**, 2542–2551.
- Xu, H., Liu, X., George, M.N., et al. (2021). Black phosphorus incorporation modulates nanocomposite hydrogel properties and subsequent MC3T3 cell attachment, proliferation, and differentiation. *J. Biomed. Mater. Res.* **109**, 1633–1645.
- Pan, C., Liu, L., and Gai, G. (2017). Recent progress of graphene-containing polymer hydrogels: preparations, properties, and applications. *Macromol. Mater. Eng.* **302**, 1700184.
- Du, G., Nie, L., Gao, G., et al. (2015). Tough and biocompatible hydrogels based on in situ interpenetrating networks of dithiol-connected graphene oxide and poly(vinyl alcohol). *ACS Appl. Mater. Interfaces* **7**, 3003–3008.
- Cong, H.P., Wang, P., and Yu, S.H. (2014). Highly elastic and superstretchable graphene oxide/polyacrylamide hydrogels. *Small* **10**, 448–453.
- Zhong, M., Liu, Y.T., and Xie, X.M. (2015). Self-healable, super tough graphene oxide-poly(acrylic acid) nanocomposite hydrogels facilitated by dual cross-linking effects through dynamic ionic interactions. *J. Mater. Chem. B* **3**, 4001–4008.
- Mao, C., Xiang, Y., Liu, X., et al. (2018). Repeatable photodynamic therapy with triggered signaling pathways of fibroblast cell proliferation and differentiation to promote bacteria-accompanied wound healing. *ACS Nano* **12**, 1747–1759.
- Shao, J., Ruan, C., Xie, H., et al. (2020). Photochemical activity of black phosphorus for near-infrared light controlled in situ biomineralization. *Adv. Sci.* **7**, 2000439.
- Liu, J., Chen, C., He, C., et al. (2012). Synthesis of graphene peroxide and its application in fabricating super extensible and highly resilient nanocomposite hydrogels. *ACS Nano* **6**, 8194–8202.
- Li, D., Müller, M.B., Gilje, S., et al. (2008). Processable aqueous dispersions of graphene nanosheets. *Nat. Nanotechnol.* **3**, 101–105.

64. Yang, X., Qiu, L., Cheng, C., et al. (2011). Ordered gelation of chemically converted graphene for next-generation electroconductive hydrogel films. *Angew. Chem. Int. Ed. Engl.* **50**, 7325–7328.
65. Mei, J., Zhang, Y., Liao, T., et al. (2019). Black phosphorus nanosheets promoted 2D-TiO₂-2D heterostructured anode for high-performance lithium storage. *Energy Storage Mater.* **19**, 424–431.
66. Li, L., Wang, C., Huang, Q., et al. (2018). A degradable hydrogel formed by dendrimer-encapsulated platinum nanoparticles and oxidized dextran for repeated photothermal cancer therapy. *J. Mater. Chem. B* **6**, 2474–2480.
67. Nishat, Z.S., Hossain, T., Islam, M.N., et al. (2022). Hydrogel nanoarchitectonics: an evolving paradigm for ultrasensitive biosensing. *Small* **18**, e2107571.
68. Li, S., Yang, Y., Wang, S., et al. (2022). Advances in metal graphitic nanocapsules for biomedicine. *Exploration* **1**, 20210223.
69. Wang, Y., Chen, L., Tan, L., et al. (2014). PEG–PCL based micelle hydrogels as oral docetaxel delivery systems for breast cancer therapy. *Biomaterials* **35**, 6972–6985.
70. Wang, X., and Wang, Q. (2021). Enzyme-laden bioactive hydrogel for biocatalytic monitoring and regulation. *Acc. Chem. Res.* **54**, 1274–1287.
71. Ikeda, M., Tanida, T., Yoshii, T., et al. (2014). Installing logic-gate responses to a variety of biological substances in supramolecular hydrogel–enzyme hybrids. *Nat. Chem.* **6**, 511–518.
72. Dannert, C., Stokke, B.T., and Dias, R.S. (2019). Nanoparticle-hydrogel composites: from molecular interactions to macroscopic behavior. *Polymers* **11**, 275.
73. Bai, H., Li, C., Wang, X., and Shi, G. (2010). A pH-sensitive graphene oxide composite hydrogel. *Chem. Commun.* **46**, 2376–2378.
74. Jiao, T., Zhao, H., Zhou, J., et al. (2015). Self-assembly reduced graphene oxide nanosheet hydrogel fabrication by anchorage of chitosan/silver and its potential efficient application toward dye degradation for wastewater treatments. *ACS Sustain. Chem. Eng.* **3**, 3130–3139.
75. Jayakumar, A., Jose, V.K., and Lee, J. (2020). Hydrogels for medical and environmental applications. *Small Methods* **4**, 1900735.
76. Zhang, K., Feng, Q., Fang, Z., et al. (2021). Structurally dynamic hydrogels for biomedical applications: pursuing a fine balance between macroscopic stability and microscopic dynamics. *Chem. Rev.* **121**, 11149–11193.
77. Zhang, Y.Z., El-Demellawi, J.K., Jiang, Q., et al. (2020). MXene hydrogels: fundamentals and applications. *Chem. Soc. Rev.* **49**, 7229–7251.
78. Chaves, A., Azadani, J.G., Alsalmán, H., et al. (2020). Bandgap engineering of two-dimensional semiconductor materials. *npj 2D Mater. Appl.* **4**, 29.
79. Wang, Z.-Q., Lü, T.-Y., Wang, H.-Q., et al. (2019). Review of borophene and its potential applications. *Front. Phys.* **14**, 33403.
80. Tai, G., Xu, M., Hou, C., et al. (2021). Borophene nanosheets as high-efficiency catalysts for the hydrogen evolution reaction. *ACS Appl. Mater. Interfaces* **13**, 60987–60994.
81. Mannix, A.J., Zhou, X.F., Kiraly, B., et al. (2015). Synthesis of borophenes: anisotropic, two-dimensional boron polymorphs. *Science* **350**, 1513–1516.
82. Wang, X., Wu, R., Xu, T., and Gao, Y. (2021). Mechanical and electrical properties of borophene and its band structure modulation via strain and electric fields: a first-principles study. *Mater. Res. Express* **8**, 065003.
83. Kochat, V., Samanta, A., Zhang, Y., et al. (2018). Atomically thin gallium layers from solid-melt exfoliation. *Sci. Adv.* **4**, e1701373.
84. Gutiérrez, Y., García-Fernández, P., Junquera, J., et al. (2020). Polymorphic gallium for active resonance tuning in photonic nanostructures: from bulk gallium to two-dimensional (2D) gallenene. *Nanophotonics* **9**, 4233–4252.
85. Petrov, M., Bekaert, J., and Milošević, M.V. (2021). Superconductivity in gallenene. *2D Mater.* **8**, 035056.
86. Yang, K., Wan, J., Zhang, S., et al. (2012). The influence of surface chemistry and size of nanoscale graphene oxide on photothermal therapy of cancer using ultra-low laser power. *Biomaterials* **33**, 2206–2214.
87. Li, Z., Kan, A., Wang, K., et al. (2022). Optical properties and photothermal conversion performances of graphene based nanofluids. *Appl. Therm. Eng.* **203**, 117948.
88. Gao, Y., Ma, D., Wang, C., et al. (2011). Reduced graphene oxide as a catalyst for hydrogenation of nitrobenzene at room temperature. *Chem. Commun.* **47**, 2432–2434.
89. Su, C., Acik, M., Takai, K., et al. (2012). Probing the catalytic activity of porous graphene oxide and the origin of this behaviour. *Nat. Commun.* **3**, 1298.
90. Lin, H., Qiu, W., Liu, J., et al. (2019). Silicene: wet-chemical exfoliation synthesis and biodegradable tumor nanomedicine. *Adv. Mater.* **31**, e1903013.
91. Ni, Z., Liu, Q., Tang, K., et al. (2012). Tunable bandgap in silicene and germanene. *Nano Lett.* **12**, 113–118.
92. Zhou, S., Pei, W., Zhao, J., and Du, A. (2019). Silicene catalysts for CO₂ hydrogenation: the number of layers controls selectivity. *Nanoscale* **11**, 7734–7743.
93. Morrissey, C., and He, H. (2018). Silicene catalyzed reduction of nitrobenzene to aniline: a mechanistic study. *Chem. Phys. Lett.* **695**, 228–234.
94. Vogt, P., Capiod, P., Berthe, M., et al. (2014). Synthesis and electrical conductivity of multilayer silicene. *Appl. Phys. Lett.* **104**, 021602.
95. Ge, M., Zong, M., Xu, D., et al. (2021). Freestanding germanene nanosheets for rapid degradation and photothermal conversion. *Mater. Today Nano* **15**, 100119.
96. Dávila, M.E., Xian, L., Cahangirov, S., et al. (2014). Germanene: a novel two-dimensional germanium allotrope akin to graphene and silicene. *New J. Phys.* **16**, 095002.
97. Bouša, D., Marvan, P., Kosina, J., et al. (2021). Picric acid violet light assisted photodegradation mediated by germanene-based materials. *Bull. Chem. Soc. Jpn.* **94**, 1695–1701.
98. Zhang, L., Bampoulis, P., van Houselt, A., and Zandvliet, H.J.W. (2015). Two-dimensional Dirac signature of germanene. *Appl. Phys. Lett.* **107**, 111605.
99. Chen, Q., Liang, L., Potsi, G., et al. (2019). Highly conductive metallic state and strong spin-orbit interaction in annealed germanene. *Nano Lett.* **19**, 1520–1526.
100. Ouyang, J., Zhang, L., Li, L., et al. (2021). Cryogenic exfoliation of 2D stanene nanosheets for cancer theranostics. *Nano-Micro Lett.* **13**, 90.
101. Ezawa, M. (2015). Monolayer topological insulators: silicene, germanene, and stanene. *J. Phys. Soc. Jpn.* **84**, 121003.
102. Yang, J., Johnson Goh, K.E., Yu, Z.G., et al. (2021). A first-principles study on strain engineering of monolayer stanene for enhanced catalysis of CO₂ reduction. *Chemosphere* **268**, 129317.
103. Xiong, W., Xia, C., Wang, T., et al. (2016). Strain and spin–orbital coupling effects on electronic structures and magnetism of semi-hydrogenated stanene. *J. Phys. Chem. C* **120**, 10622–10628.
104. Shao, J., Xie, H., Huang, H., et al. (2016). Biodegradable black phosphorus-based nanospheres for in vivo photothermal cancer therapy. *Nat. Commun.* **7**, 12967.
105. Jiang, Q., Xu, L., Chen, N., et al. (2016). Facile synthesis of black phosphorus: an efficient electrocatalyst for the oxygen evolving reaction. *Angew. Chem. Int. Ed. Engl.* **55**, 13849–13853.
106. Batmunkh, M., Myekhlai, M., Bati, A.S.R., et al. (2019). Microwave-assisted synthesis of black phosphorus quantum dots: efficient electrocatalyst for oxygen evolution reaction. *J. Mater. Chem.* **7**, 12974–12978.
107. Chen, W., Ouyang, J., Liu, H., et al. (2017). Black phosphorus nanosheet-based drug delivery system for synergistic photodynamic/photothermal/chemotherapy of cancer. *Adv. Mater.* **29**, 1603864.
108. Li, Z., Zhang, T., Fan, F., et al. (2020). Piezoelectric materials as sonodynamic sensitizers to safely ablate tumors: a case study using black phosphorus. *J. Phys. Chem. Lett.* **11**, 1228–1238.
109. Fei, R., Faghaninia, A., Soklaski, R., et al. (2014). Enhanced thermoelectric efficiency via orthogonal electrical and thermal conductances in phosphorene. *Nano Lett.* **14**, 6393–6399.
110. Kong, N., Zhang, H., Feng, C., et al. (2021). Arsenene-mediated multiple independently targeted reactive oxygen species burst for cancer therapy. *Nat. Commun.* **12**, 4777.
111. Zhang, S., Yan, Z., Li, Y., et al. (2015). Atomically thin arsenene and antimonene: semimetal-semiconductor and indirect-direct band-gap transitions. *Angew. Chem. Int. Ed. Engl.* **54**, 3112–3115.
112. Liu, J., Hinsch, J.J., Yin, H., et al. (2022). β -arsenene monolayer: a promising electrocatalyst for anodic chlorine evolution reaction. *Catalysts* **12**, 296.
113. Pizzi, G., Gibertini, M., Dib, E., et al. (2016). Performance of arsenene and antimonene double-gate MOSFETs from first principles. *Nat. Commun.* **7**, 12585.
114. Xue, C.-L., and Li, S.-C. (2021). Recent progress on antimonene: from theoretical calculation to epitaxial growth. *Jpn. J. Appl. Phys.* **60**, SE0805.
115. Ji, J., Song, X., Liu, J., et al. (2016). Two-dimensional antimonene single crystals grown by van der Waals epitaxy. *Nat. Commun.* **7**, 13352.
116. Kang, Y., Li, Z., Yang, Y., et al. (2021). Antimonene nanosheets-based Z-scheme heterostructure with enhanced reactive oxygen species generation and photothermal conversion efficiency for photonic therapy of cancer. *Adv. Healthc. Mater.* **10**, e2001835.
117. Bat-Erdene, M., Xu, G., Batmunkh, M., et al. (2020). Surface oxidized two-dimensional antimonene nanosheets for electrochemical ammonia synthesis under ambient conditions. *J. Mater. Chem.* **8**, 4735–4739.
118. Wang, G., Ding, Y., Guan, Y., et al. (2022). Tunable electronic properties of few-layer tellurene under in-plane and out-of-plane uniaxial strain. *Nanomaterials* **12**, 875.
119. Zhu, Y., Wu, Y., Li, S., et al. (2022). Photocatalytic and photothermal bismuthene nanosheets as drug carrier capable of generating CO to improve drug sensitivity and reduce inflammation for enhanced cancer therapy. *Chem. Eng. J.* **446**, 137321.
120. Bhuvaneshwari, R., Nagarajan, V., and Chandiramouli, R. (2019). Electronic properties of novel bismuthene nanosheets with adsorption studies of G-series nerve agent molecules—a DFT outlook. *Phys. Lett.* **383**, 125975.
121. Cao, C., Ma, D.D., Gu, J.F., et al. (2020). Metal-organic layers leading to atomically thin bismuthene for efficient carbon dioxide electroreduction to liquid fuel. *Angew. Chem. Int. Ed. Engl.* **59**, 15014–15020.
122. Cheng, L., Liu, H., Tan, X., et al. (2013). Thermoelectric properties of a monolayer bismuth. *J. Phys. Chem. C* **118**, 904–910.
123. Sakr, T.M., Korany, M., and Katti, K.V. (2018). Selenium nanomaterials in biomedicine—an overview of new opportunities in nanomedicine of selenium. *J. Drug Deliv. Sci. Technol.* **46**, 223–233.
124. Lin, C., Cheng, W., Chai, G., and Zhang, H. (2018). Thermoelectric properties of two-dimensional selenene and tellurene from group-VI elements. *Phys. Chem. Chem. Phys.* **20**, 24250–24256.
125. Pan, W., Liu, C., Li, Y., et al. (2022). Ultrathin tellurium nanosheets for simultaneous cancer thermo-chemotherapy. *Bioact. Mater.* **13**, 96–104.
126. Wu, B., Liu, X., Yin, J., and Lee, H. (2017). Bulk β -Te to few layered β -tellurenes: indirect to direct band-gap transitions showing semiconducting property. *Mater. Res. Express* **4**, 095902.
127. Zhao, Y., Wang, H., Huang, H., et al. (2016). Surface coordination of black phosphorus for robust air and water stability. *Angew. Chem. Int. Ed. Engl.* **55**, 5003–5007.
128. Liu, C., Sun, S., Feng, Q., et al. (2021). Arsenene Nanodots with Selective Killing Effects and their Low-Dose Combination with β -Element for Cancer Therapy. *Adv. Mater.* **33**, 2102054.

129. Tao, W., Kong, N., Ji, X., et al. (2019). Emerging two-dimensional mono-elemental materials (Xenes) for biomedical applications. *Chem. Soc. Rev.* **48**, 2891–2912.
130. Liu, H., Neal, A.T., Zhu, Z., et al. (2014). Phosphorene: an unexplored 2D semiconductor with a high hole mobility. *ACS Nano* **8**, 4033–4041.
131. Qiao, J., Kong, X., Hu, Z.X., et al. (2014). High-mobility transport anisotropy and linear dichroism in few-layer black phosphorus. *Nat. Commun.* **5**, 4475.
132. Li, L., Yu, Y., Ye, G.J., et al. (2014). Black phosphorus field-effect transistors. *Nat. Nanotechnol.* **9**, 372–377.
133. Zou, Y., Chen, X., Yang, P., et al. (2020). Regulating the absorption spectrum of polydopamine. *Sci. Adv.* **6**, eabb4696.
134. Kou, L., Ma, Y., Sun, Z., et al. (2017). Two-dimensional topological insulators: progress and prospects. *J. Phys. Chem. Lett.* **8**, 1905–1919.
135. Ou, M., Wang, X., Yu, L., et al. (2021). The emergence and evolution of borophene. *Adv. Sci.* **8**, 2001801.
136. Rizwan, M., Yahya, R., Hassan, A., et al. (2017). pH sensitive hydrogels in drug delivery: brief history, properties, swelling, and release mechanism, material selection and applications. *Polymers* **9**, E225.
137. He, B., Wang, Y., Zhai, Q., et al. (2020). From polymeric carbon nitride to carbon materials: extended application to electrochemical energy conversion and storage. *Nanoscale* **12**, 8636–8646.
138. Ji, T., Niu, T., Wang, J., et al. (2022). Crystallization regulation of solution-processed two-dimensional perovskite solar cells. *J. Mater. Chem.* **10**, 13625–13650.
139. Shen, J., Yan, B., Li, T., et al. (2012). Mechanical, thermal and swelling properties of poly(acrylic acid)-graphene oxide composite hydrogels. *Soft Matter* **8**, 1831–1836.
140. Zhang, N., Li, R., Zhang, L., et al. (2011). Actuator materials based on graphene oxide/polyacrylamide composite hydrogels prepared by in situ polymerization. *Soft Matter* **7**, 7231.
141. Guiseppi-Elie, A. (2010). Electroconductive hydrogels: synthesis, characterization and biomedical applications. *Biomaterials* **31**, 2701–2716.
142. Liu, Y., Xiao, Y., Cao, Y., et al. (2020). Construction of chitosan-based hydrogel incorporated with antimonene nanosheets for rapid capture and elimination of bacteria. *Adv. Funct. Mater.* **30**, 2003196.
143. Pan, W., Dai, C., Li, Y., et al. (2020). PRP-chitosan thermoresponsive hydrogel combined with black phosphorus nanosheets as injectable biomaterial for biotherapy and phototherapy treatment of rheumatoid arthritis. *Biomaterials* **239**, 119851.
144. Wang, Y., Qiu, M., Won, M., et al. (2019). Emerging 2D material-based nanocarrier for cancer therapy beyond graphene. *Coord. Chem. Rev.* **400**, 213041.
145. Gu, Z., Zhu, S., Yan, L., et al. (2019). Graphene-based smart platforms for combined cancer therapy. *Adv. Mater.* **31**, e1800662.
146. Hu, T., Mei, X., Wang, Y., et al. (2019). Two-dimensional nanomaterials: fascinating materials in biomedical field. *Sci. Bull.* **64**, 1707–1727.
147. Lee, T.H., Kim, S.Y., and Jang, H.W. (2016). Black phosphorus: critical review and potential for water splitting photocatalyst. *Nanomaterials* **6**, 194.
148. Koehler, J., Brandl, F.P., and Goepferich, A.M. (2018). Hydrogel wound dressings for bioactive treatment of acute and chronic wounds. *Eur. Polym. J.* **100**, 1–11.
149. Xie, J., Fan, T., Kim, J.H., et al. (2020). Emetine-loaded black phosphorus hydrogel sensitizes tumor to photothermal therapy through inhibition of stress granule formation. *Adv. Funct. Mater.* **30**, 2003891.
150. Qin, L., Ling, G., Peng, F., et al. (2019). Black phosphorus nanosheets and gemcitabine encapsulated thermo-sensitive hydrogel for synergistic photothermal-chemotherapy. *J. Colloid Interface Sci.* **556**, 232–238.
151. Lu, J., He, Y.-S., Cheng, C., et al. (2013). Self-supporting graphene hydrogel film as an experimental platform to evaluate the potential of graphene for bone regeneration. *Adv. Funct. Mater.* **23**, 3494–3502.
152. Huang, K., Wu, J., and Gu, Z. (2019). Black phosphorus hydrogel scaffolds enhance bone regeneration via a sustained supply of calcium-free phosphorus. *ACS Appl. Mater. Interfaces* **11**, 2908–2916.
153. Liu, X., George, M.N., Li, L., et al. (2020). Injectable electrical conductive and phosphate releasing gel with two-dimensional black phosphorus and carbon nanotubes for bone tissue engineering. *ACS Biomater. Sci. Eng.* **6**, 4653–4665.
154. Paul, A., Hasan, A., Kindi, H.A., et al. (2014). Injectable graphene oxide/hydrogel-based angiogenic gene delivery system for vasculogenesis and cardiac repair. *ACS Nano* **8**, 8050–8062.
155. Annabi, N., Shin, S.R., Tamayol, A., et al. (2016). Highly elastic and conductive human-based protein hybrid hydrogels. *Adv. Mater.* **28**, 40–49.
156. Ouyang, J., Ji, X., Zhang, X., et al. (2020). In situ sprayed NIR-responsive, analgesic black phosphorus-based gel for diabetic ulcer treatment. *Proc. Natl. Acad. Sci. USA* **117**, 28667–28677.
157. Singh, N., Ali, M.A., Rai, P., et al. (2020). Dual-modality microfluidic biosensor based on nanoengineered mesoporous graphene hydrogels. *Lab Chip* **20**, 760–777.
158. Li, P., Jin, Z., Peng, L., et al. (2018). Stretchable all-gel-state fiber-shaped supercapacitors enabled by macromolecularly interconnected 3D graphene/nanostructured conductive polymer hydrogels. *Adv. Mater.* **30**, e1800124.
159. Gao, M., Peh, C.K.N., Ong, W.L., and Ho, G.W. (2013). Green chemistry synthesis of a nano-composite graphene hydrogel with three-dimensional nano-mesopores for photocatalytic H₂ production. *RSC Adv.* **3**, 13169.
160. Wang, R., Zhang, M., Ge, B., et al. (2020). Facile preparation of black phosphorus-based rGO-BP-Pd composite hydrogels with enhanced catalytic reduction of 4-nitrophenol performances for wastewater treatment. *J. Mol. Liq.* **310**, 113083.
161. Zhao, Y., Zhang, Z., Pan, Z., and Liu, Y. (2021). Advanced bioactive nanomaterials for biomedical applications. *Exploration* **1**, 20210089.
162. Ali, F., Khan, I., Chen, J., et al. (2022). Emerging fabrication strategies of hydrogels and its applications. *Gels* **8**, 205.
163. Luo, M., Fan, T., Zhou, Y., et al. (2019). 2D black phosphorus-based biomedical applications. *Adv. Funct. Mater.* **29**, 1808306.
164. Zeng, X., Luo, M., Liu, G., et al. (2018). Polydopamine-modified black phosphorous nanocapsule with enhanced stability and photothermal performance for tumor multimodal treatments. *Adv. Sci.* **5**, 1800510.
165. Dong, Y., Li, S., Li, X., and Wang, X. (2021). Smart MXene/agarose hydrogel with photothermal property for controlled drug release. *Int. J. Biol. Macromol.* **190**, 693–699.
166. Shin, S.R., Li, Y.C., Jang, H.L., et al. (2016). Graphene-based materials for tissue engineering. *Adv. Drug Deliv. Rev.* **105**, 255–274.
167. Qiu, M., Wang, D., Liang, W., et al. (2018). Novel concept of the smart NIR-light-controlled drug release of black phosphorus nanostructure for cancer therapy. *Proc. Natl. Acad. Sci. USA* **115**, 501–506.
168. Ma, J., and Wu, C. (2022). Bioactive inorganic particles-based biomaterials for skin tissue engineering. *Exploration* **1**, 20210083.
169. Shi, X., Chang, H., Chen, S., et al. (2012). Regulating cellular behavior on few-layer reduced graphene oxide films with well-controlled reduction states. *Adv. Funct. Mater.* **22**, 751–759.
170. Zhang, Z., Zhou, J., Liu, C., et al. (2022). Emerging Biomimetic Nanotechnology in Orthopedic Diseases: Progress, Challenges, and Opportunities. *Trends Chem* **4**, 420–436.
171. Zhou, J., Zhang, Z., Joseph, J., et al. (2021). Biomaterials and Nanomedicine for Bone Regeneration: Progress and Future Prospects. *Exploration* **1**, 20210011.
172. Zhang, X., Koo, S., Kim, J.H., et al. (2021). Nanoscale Materials-Based Platforms for the Treatment of Bone-Related Diseases. *Matter* **4**, 2727–2764.
173. Nayak, T.R., Andersen, H., Makam, V.S., et al. (2011). Graphene for controlled and accelerated osteogenic differentiation of human mesenchymal stem cells. *ACS Nano* **5**, 4670–4678.
174. Mohammadrezaei, D., Golzar, H., Rezaei Rad, M., et al. (2018). In vitro effect of graphene structures as an osteoinductive factor in bone tissue engineering: a systematic review. *J. Biomed. Mater. Res.* **106**, 2284–2343.
175. Lee, W.C., Lim, C.H.Y.X., Shi, H., et al. (2011). Origin of enhanced stem cell growth and differentiation on graphene and graphene oxide. *ACS Nano* **5**, 7334–7341.
176. Saravanan, S., Vimalraj, S., and Anuradha, D. (2018). Chitosan based thermoresponsive hydrogel containing graphene oxide for bone tissue repair. *Biomed. Pharmacother.* **107**, 908–917.
177. Dvir, T., Timko, B.P., Brigham, M.D., et al. (2011). Nanowired three-dimensional cardiac patches. *Nat. Nanotechnol.* **6**, 720–725.
178. Shin, S.R., Aghaei-Ghareh-Bolagh, B., Gao, X., et al. (2014). Layer-by-layer assembly of 3D tissue constructs with functionalized graphene. *Adv. Funct. Mater.* **24**, 6136–6144.
179. Alagarsamy, K.N., Mathan, S., Yan, W., et al. (2021). Carbon nanomaterials for cardiovascular therapeutics: promises and challenges. *Bioact. Mater.* **6**, 2261–2280.
180. Terry, L.A., White, S.F., and Tigwell, L.J. (2005). The application of biosensors to fresh produce and the wider food industry. *J. Agric. Food Chem.* **53**, 1309–1316.
181. Lim, J.Y.C., Goh, S.S., and Loh, X.J. (2020). Bottom-Up engineering of responsive hydrogel materials for molecular detection and biosensing. *ACS Mater. Lett.* **2**, 918–950.
182. Li, Y., Huang, Z.Z., Weng, Y., and Tan, H. (2019). Pyrophosphate ion-responsive alginate hydrogel as an effective fluorescent sensing platform for alkaline phosphatase detection. *Chem. Commun.* **55**, 11450–11453.
183. Alim, S., Vejjayan, J., Yusoff, M.M., and Kafi, A.K.M. (2018). Recent uses of carbon nanotubes & gold nanoparticles in electrochemistry with application in biosensing: a review. *Biosens. Bioelectron.* **121**, 125–136.
184. Song, H.S., Kwon, O.S., Kim, J.H., et al. (2017). 3D hydrogel scaffold doped with 2D graphene materials for biosensors and bioelectronics. *Biosens. Bioelectron.* **89**, 187–200.
185. Gawel, K., Barriet, D., Sletmoen, M., and Stokke, B.T. (2010). Responsive hydrogels for label-free signal transduction within biosensors. *Sensors* **10**, 4381–4409.
186. Wang, Y., Brunsen, A., Jonas, U., et al. (2009). Prostate specific antigen biosensor based on long range surface plasmon-enhanced fluorescence spectroscopy and dextran hydrogel binding matrix. *Anal. Chem.* **81**, 9625–9632.
187. Tavakoli, J., and Tang, Y. (2017). Hydrogel based sensors for biomedical applications: an updated review. *Polymers* **9**, 364.
188. Zhang, X., Pan, S., Song, H., et al. (2021). Photothermal effect enables markedly enhanced oxygen reduction and evolution activities for high-performance Zn-air batteries. *J. Mater. Chem.* **9**, 19734–19740.
189. Wang, Z., Li, H., Tang, Z., et al. (2018). Hydrogel electrolytes for flexible aqueous energy storage devices. *Adv. Funct. Mater.* **28**, 1804560.
190. Li, Q., Mahendra, S., Lyon, D.Y., et al. (2008). Antimicrobial nanomaterials for water disinfection and microbial control: potential applications and implications. *Water Res.* **42**, 4591–4602.
191. Alvarez, P.J.J., Chan, C.K., Elimelech, M., et al. (2018). Emerging opportunities for nanotechnology to enhance water security. *Nat. Nanotechnol.* **13**, 634–641.
192. Zeng, X., Wang, G., Liu, Y., and Zhang, X. (2017). Graphene-based antimicrobial nanomaterials: rational design and applications for water disinfection and microbial control. *Environ. Sci. Nano* **4**, 2248–2266.
193. Guo, Y., Bae, J., Fang, Z., et al. (2020). Hydrogels and hydrogel-derived materials for energy and water sustainability. *Chem. Rev.* **120**, 7642–7707.
194. Raafat, D., Von Bargen, K., Haas, A., and Sahl, H.G. (2008). Insights into the mode of action of chitosan as an antibacterial compound. *Appl. Environ. Microbiol.* **74**, 3764–3773.

195. Guo, Y., Dundas, C.M., Zhou, X., et al. (2021). Molecular engineering of hydrogels for rapid water disinfection and sustainable solar vapor generation. *Adv. Mater.* **33**, e2102994.
196. Mauter, M.S., Zucker, I., Perreault, F., et al. (2018). The role of nanotechnology in tackling global water challenges. *Nat. Sustain.* **1**, 166–175.
197. Fan, Y., Ma, W., Han, D., et al. (2015). Convenient recycling of 3D AgX/graphene aerogels (X = Br, Cl) for efficient photocatalytic degradation of water pollutants. *Adv. Mater.* **27**, 3767–3773.
198. Lu, K.-Q., Xin, X., Zhang, N., et al. (2018). Photoredox catalysis over graphene aerogel-supported composites. *J. Mater. Chem.* **6**, 4590–4604.
199. Wan, W., Yu, S., Dong, F., et al. (2016). Efficient C_3N_4 /graphene oxide macroscopic aerogel visible-light photocatalyst. *J. Mater. Chem.* **4**, 7823–7829.
200. Zhao, Z., Fang, R., Rong, Q., and Liu, M. (2017). Bioinspired nanocomposite hydrogels with highly ordered structures. *Adv. Mater.* **29**, 1703045.
201. Kim, H.N., Jiao, A., Hwang, N.S., et al. (2013). Nanotopography-guided tissue engineering and regenerative medicine. *Adv. Drug Deliv. Rev.* **65**, 536–558.
202. Caliani, S.R., and Burdick, J.A. (2016). A practical guide to hydrogels for cell culture. *Nat. Methods* **13**, 405–414.
203. Zhao, Y., Zeng, H., Nam, J., and Agarwal, S. (2009). Fabrication of skeletal muscle constructs by topographic activation of cell alignment. *Biotechnol. Bioeng.* **102**, 624–631.
204. Boote, C., Dennis, S., Huang, Y., et al. (2005). Lamellar orientation in human cornea in relation to mechanical properties. *J. Struct. Biol.* **149**, 1–6.
205. Keene, D.R., Engvall, E., and Glanville, R.W. (1988). Ultrastructure of type VI collagen in human skin and cartilage suggests an anchoring function for this filamentous network. *J. Cell Biol.* **107**, 1995–2006.
206. Yang, F., Li, J., Long, Y., et al. (2021). Wafer-scale heterostructured piezoelectric bio-organic thin films. *Science* **373**, 337–342.
207. Cho, J., and Ishida, Y. (2017). Macroscopically oriented porous materials with periodic ordered structures: from zeolites and metal-organic frameworks to liquid-crystal-templated mesoporous materials. *Adv. Mater.* **29**, 1605974.
208. Maggini, L., Liu, M., Ishida, Y., and Bonifazi, D. (2013). Anisotropically luminescent hydrogels containing magnetically-aligned MWCNTs-Eu(III) hybrids. *Adv. Mater.* **25**, 2462–2467.
209. Matsuura, T., Wada, T., Tatewaki, Y., and Okada, S. (2014). Effective polar orientation of organic polar nanocrystals and their fixation in polymer matrices. *Jpn. J. Appl. Phys.* **53**, 061601.
210. Kim, J.E., Han, T.H., Lee, S.H., et al. (2011). Graphene oxide liquid crystals. *Angew. Chem. Int. Ed. Engl.* **50**, 3043–3047.
211. Downes, R., Wang, S., Haldane, D., et al. (2015). Strain-induced alignment mechanisms of carbon nanotube networks. *Adv. Eng. Mater.* **17**, 349–358.
212. Lin, P., Zhang, T., Wang, X., et al. (2016). Freezing molecular orientation under stretch for high mechanical strength but anisotropic hydrogels. *Small* **12**, 4386–4392.
213. Choi, S., and Kim, J. (2015). Designed fabrication of super-stiff, anisotropic hybrid hydrogels via linear remodeling of polymer networks and subsequent crosslinking. *J. Mater. Chem. B* **3**, 1479–1483.
214. Lei, Z., Wang, Q., Sun, S., et al. (2017). A bioinspired mineral hydrogel as a self-healable, mechanically adaptable ionic skin for highly sensitive pressure sensing. *Adv. Mater.* **29**, 1700321.
215. Fu, R., Tu, L., Zhou, Y., et al. (2019). A tough and self-powered hydrogel for artificial skin. *Chem. Mater.* **31**, 9850–9860.
216. Low, Z.W.K., Li, Z., Owh, C., et al. (2020). Recent innovations in artificial skin. *Biomater. Sci.* **8**, 776–797.
217. Gogurla, N., Roy, B., and Kim, S. (2020). Self-powered artificial skin made of engineered silk protein hydrogel. *Nano Energy* **77**, 105242.
218. Ryplida, B., Lee, K.D., Park, S.Y., and In, I. (2019). Light-induced swelling-responsive conductive, adhesive, and stretchable wireless film hydrogel as electronic artificial skin. *Adv. Funct. Mater.* **29**, 1903209.
219. Nie, C., Ma, L., Li, S., et al. (2019). Recent progresses in graphene based bio-functional nanostructures for advanced biological and cellular interfaces. *Nano Today* **26**, 57–97.

ACKNOWLEDGMENTS

This study was financially supported by a grant from the National Natural Science Foundation of China (Grant No. 32071322; to X.J.), National Natural Science Foundation of China for Excellent Young Scholar (Grant No. 32122044; to X.J.), and the Technology & Innovation Commission of Shenzhen Municipality (Grant No. JCYJ20210324113004010; to X.J.). W.T. acknowledges the supports from American Heart Association Collaborative Science Award (No. 2018A004190; to W.T.), Harvard Medical School/Brigham and Women's Hospital Department of Anesthesiology-Basic Scientist Grant (No. 2420 BPA075; to W.T.), Nanotechnology Foundation (No. 2022A002721; to W.T.), Gillian Reny Stepping Strong Center for Trauma Innovation Breakthrough Innovator Award (No. 113548; to W.T.), Center for Nanomedicine Research Fund (No. 2019A014810; to W.T.), Khoury Innovation Award (No. 2020A003219; to W.T.), and Farokhzad Family Distinguished Chair Foundation (No. 018129; to W.T.).

AUTHOR CONTRIBUTIONS

W.T., X.J., and C.F. supervised and organized the review. Y.K. and H.Z. designed and wrote the manuscript. L.C., J.D., B.Y., X.Y., D.Q., A.Y., and C.L. gave suggestions of conceptual ideas and revised the manuscript. All authors read and approved the manuscript.

DECLARATION OF INTERESTS

The authors declare no competing interests.

LEAD CONTACT WEBSITE

<http://mctu.tju.edu.cn/info/1193/1564.htm>.